



Distant Monitoring of Entangled Macro-Objects

Serge Kernbach*

ABSTRACT

The paper discusses application of long-range signal transmission system for distant monitoring of entangled macro-objects. The approach is based on electrochemical impedance spectroscopy with optical excitation within the framework of weak macroscopic entanglement. The 'activity index' is introduced as a characteristic of distant objects and its meaning is analysed for different experimental and environmental conditions. Probabilistic parameters of non-local measurements, methods for increasing their reproducibility and reliability, as well as various configurations of the measuring system are described. The results of calibration and control experiments with geographic, physical, biological and symbolic objects are represented. The system enables testing entangled macro-objects on possessing specific features/properties measured by multiple devices in parallel. Distant monitoring can be used as part of a system conducting interactions with biological objects, as well as for independent usage as diagnostic or surveillance equipment.

DOI Number: 10.14704/nq.2019.17.03.1977

NeuroQuantology 2019; 17(03):19-42

Introduction

Multiple works (Akimov *et al.*, 2001), (Maslobrod *et al.*, 2014a), (Kernbach *et al.*, 2016), (Smirnov, 2010) are devoted to the effect of non-local signal transmission. This effect is related to macroscopic entanglement (ME) (Palomaki *et al.*, 2013), (Sperling and Walmsley, 2017), (Ockeloen-Korppi *et al.*, 2018), (Vedral, 2008) and can be considered from several points of view: 1) as the ability to transmit signals between remote macro-systems; 2) to impose a non-local impact on a certain object; 3) to monitor remote objects. Most of technical papers are devoted to 1) and 2), in the area of distant monitoring it needs to mention early works (Russell, 1997), Soviet and US research (Ochatrin *et al.*, 1997), (Akimov *et al.*, 2000), (Dunne *et al.*, 1988), and teams operating with RNG devices (Hirukawa and Ishikawa, 2004), (Radin, 2002), (Nelson *et al.*, 1995); from the last 20 years – the works (Shkatov, 2010), (Kravchenko and Kalaschenko, 1994), (Gorbatych *et al.*, 2009), (Schmieke, 2015), companies 'InfoScan' and 'GeoScan Systems' (Glowatzki and Haeder, 2015). Operator-based phenomena, such as ESP (Hansel, 1969),

(Swann, 1987) or quantum consciousness (Persinger and Lavallee, 2010) are not considered here.

The experimentally observed effect consists in a weak behavioural correlation of two entangled macro-systems. Dynamics of the first system reflects impacts on the second system and vice versa, impacts on the first system are traced in the dynamics of the second system. For example in (Kernbach, 2017a), a plant was impacted over 3km distance, and correlations 'transmitter receiver' and 'receiver transmitter' are detected in dynamics of both the receiver (plant) and the transmitting system.

Existing remote monitoring systems represent different variations of this scheme, e.g. with 'matrices', 'resonant' filters, 'non-local' tags, satellite images and photographs of terrain or laser probes (Akimov *et al.*, 2000), (Ochatrin *et al.*, 1997), (Glowatzki, 2016), (Kernbach *et al.*, 2015). The reproducibility and reliability of these methods are not high and often depend on abilities of the operator. Therefore, the main application area lies in preliminary information analysis, narrowing down the initial range of search, or in cases when no other sources of information is

Corresponding author: Serge Kernbach

Address: *Cybertronica Research, Research Center of Advanced Robotics and Environmental Science, Melunerstr. 40, 70569 Stuttgart, Germany

e-mail ✉ serge.kernbach@cybertronica.de.com

Relevant conflicts of interest/financial disclosures: The authors declare that the research was conducted in the absence of any commercial or financial relationships that could be construed as a potential conflict of interest.

Received: 01 February 2019; **Accepted:** 28 February 2019



available. For example, minimizing the search area of mineral deposits, preliminary marking in SAR operations, restricting the area of geopathic zones, distant monitoring of biological organisms, etc. There are known rare applications of these methods in anti-terror, military or intelligence operations (Greig, 2012), (Popov, 2012), (Interfax, 2007), (Newsru, 2005), (Ptichkin, 2009), (May *et al.*, 2014). The response of academic community is polarized, although this possibility is discussed in quantum research: 'Quantum entanglement allows engineered quantum systems to exceed classical information processing bounds' (Palomaki *et al.*, 2013), especially for biological systems, neurons, and the brain (Koch and Hepp, 2006), (Jedlicka, 2017), (Cardena, 2014).

The proposed approach of distant monitoring is based on electrochemical impedance spectroscopy (EIS) with optical excitation and represents a combination of two systems published in (Kernbach, 2013b) and (Kernbach, 2017a). The method consists in creating an entangled system with remote object and aqueous solution in measurement containers. Over 1000 performed experiments, in particular with LEDs excitation at 470nm, demonstrated the non-local signal (impact) transmission between such macro-systems (Akimov *et al.*, 2001), (Kernbach, 2013a), (Kernbach *et al.*, 2016). These experiments allow expressing the hypothesis that a remote object affects the EIS dynamics of aqueous solution in presence of optical excitation. Measuring distortions of electrochemical dynamics (Kernbach *et al.*, 2017), it is possible to characterize this effect. The more 'active' is an entangled macro-object, the more intense is the deviation from undistorted state. The statistical characterization of electrochemical noise is used for numerical evaluation, which was already tested in other EIS applications (CYBRES, 2018a).

Thus, this method allows assessing the 'activity index' of a remote object – its ability to influence other objects. Performing differential measurements with two remote macro-objects enables 'feature matching' by multiple EIS devices – tests on possessing specific properties, although this approach requires further experiments. 'Activity' is manifested in two ways, it can stimulate or inhibit the dynamics of corresponding EIS channel. These changes can be expressed in terms of entropy/negentropy and related to the state of a remote object. This aspect is especially relevant for pathogenic objects/zones, allowing to determine their possible parameters without direct

contact. Experiments also demonstrated a selective detection of global 'emotional'/'cosmo-biological' events. An interesting area of research represents exploration of symbolic objects that demonstrate a certain 'activity' (Kernbach, 2018b). Totally, about 4000 measurements (60 experiments each with 8 runs by 8 or 16 devices, $6.8 \cdot 10^6$ measurement points or $5.5 \cdot 10^{10}$ data samples) are performed within this and the preliminary work (Kernbach, 2018a).

This paper has the following structure: Section 2 describes the setup and methodology, Sections 3 and 4 – experiments with various objects and 'feature matching' approach with 8 and 16 EIS devices, Section 5 concludes this work.

Setup and Methodology

Physical and biological macroscopic entanglement

One of the first exploratory work on physical ME considered spin systems and free Bosonic gases, achieving ME was associated with phase transitions (Anders and Vedral, 2007). These experiments are summarized in (Vedral, 2008) proposing universal character of ME in different macro-systems. In last 10 years the number of ME-related publications is significantly increased. For instance (Klimov *et al.*, 2015) deals with silicon chip and ME is achieved by using magnetic field with optical excitation at 975nm by 100mW laser, whereas ME is characterized by specific metric. In (Lee *et al.*, 2011) ME is achieved by optical excitation of two spatially separated, millimeter-sized diamonds. In (Wang *et al.*, 2016) ME was achieved in coupled mechanical oscillators modulated by optomechanical system. The degree of mechanical entanglement was assessed by vibrational model. The work (Ockeloen-Korppi *et al.*, 2018) deals with micromechanical oscillators, coupled by EM fields. The paper (Korotaev *et al.*, 2018) reports about strong ME achieved in electric field by weakly polarized electrodes performing underwater measurements in Baikal Lake. In fact, the list of publications on physical ME is long, authors reported about strong behavioural, structural, functional and even causal correlations/anomalies in spatially separated macro-systems.

Biological ME goes back to Schrödinger who recognized a significant role of quantum mechanics in biology. This field is currently referred to as quantum biology (Mohseni *et al.*, 2014). To provide a few examples: in (Shi *et al.*, 2017) ME is established between fluorescent proteins by optical excitation at



785nm, (Marletto *et al.*, 2018) treats green sulphur bacteria and quantised light, (Mothersill *et al.*, 2018) considers Zebra fish populations with ME achieved by X-ray radiation. X-ray radiation was used also for entangling seeds (Maslobrod, 2012), previous research indicated that EM field applied during swelling and germination phases produces ME in plant organisms (Maslobrod *et al.*, 1994), (Maslobrod *et al.*, 2004). Plants are the first biological objects that are used for 'technological ME', e.g. (Akimov *et al.*, 2001) used samples of plant tissues for ME established by excitation with orthogonal electric and magnetic fields. Characterization of ME was carried out by measuring correlations between excitation signal and response of biopotentials from spatially separated biological samples at 22km distance. This system utilized a signal correlation for transferring '0'/'1' bits and represents in fact the first telecommunication attempt based on biological ME. This experiment was positively replicated in (Kernbach, 2017a) with modern equipment.

Assessing ME as a correlation of electromagnetic signals induced by biological systems stimulated further development of these methods for achieving ME. For instance, (Montagnier *et al.*, 2011) reports about using DNA with magnetic fields and recorded EM signals, similar experiments are conducted by (Surinov, 2018) with mice, (Smirnov, 2010) describes excitation by microwave radiation at 1.9mm with images of rats, (Krasnobrygev, 2009) excites spatially distributed materials by alternating magnetic field and analyzes their interactions with biological objects, (Maslobrod *et al.*, 2014a) uses digital images and optical excitation for long-range biological ME with seeds, fungi and plant seedlings at 2000km distance, (Hachumova *et al.*, 2014) utilizes low-frequency EM fields with acoustic and video signals, experiments in (Kernbach *et al.*, 2016) are conducted by optical/electric field excitation with digital images and video signals. The list of such experiments and publications can be extended further. Several authors (Zhigalov, 2016), (Melkikh, 2013), (Ghirardi *et al.*, 1986) expressed a hypothesis about collapse of wave function for theoretical explanation of these phenomena – such an approach can be denoted as weak ME. This work follows the methodology of optical/electric field excitation and a digital representation of distant objects (denoted further as 'keys'). We point out such an approach represents an open research topic that is experimentally explored in a large community.

EIS setup and measurement methodology

The used setup represents a standard MU3.4 system with external electrodes, which have a built-in optical excitation at 470/940nm with two-frequency modulation – the high-frequency up to 12 MHz and the low-frequency up to 1 kHz. Structure and several such devices are shown see Fig. 1. Taking into account experiments with optical generators (Kernbach, 2013b), (Kernbach, 2013a), the experiments were carried out at excitation frequencies of 1 MHz/5 Hz, or without modulation, at the wavelength of 470 nm (blue LED). Electrical excitation for EIS measurements was performed at 450 Hz. MU EIS system records a large number of electrochemical, statistical and environmental data – totally 59 data channels per device (sampling interval – 1 sec.), see more in (CYBRES, 2018b).

The initial EIS dynamics depends on several factors, among them the state of electrode surface, the level of gas absorption (primarily CO₂ from the atmosphere), the difference in temperature of samples, light, etc. To unify these factors, electrodes were soaked in water for 10–15 minutes before the experiments, containers were filled with water in the same way, measurements starts after equalizing temperature in containers, the same paper was used for keys in both channels, samples were stored in the foam block during experiments, see Fig. 1(b). Since electrodes undergo a slow ions diffusion process¹, only such electrodes are selected that showed the most linear dynamics of both channels. These electrodes were used in further measurements.

Reflecting surface of keys. The reflecting surface of 'keys' (labels with printed images, installed on water containers, see Fig. 2(a)) affects the EIS dynamics with optical excitation and may represent a technological artefact in these measurements. However, as shown by experiments, the reflecting surface is not the main influencing factor on EIS dynamics. For example, images of 'stone' and 'plant', see Fig.8(a,b), have a similar amount of black color, but they demonstrate significantly different results, see Fig. 7. After a number of preliminary experiments with 'black square keys', see Fig. 8(d), the image of the object was placed on the outer side of keys, i.e. the inner reflective surface of both keys remained white, and the containers are installed in matte black

¹ Slow ions transfer from metal to aqueous solutions during the measurement process, which represents one of reasons for degradation of EIS dynamics during long-term measurements. To ensure linear dynamics of both EIS channels in the initial region, it is necessary to select electrodes.



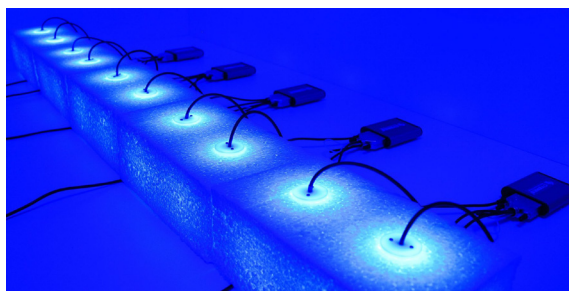
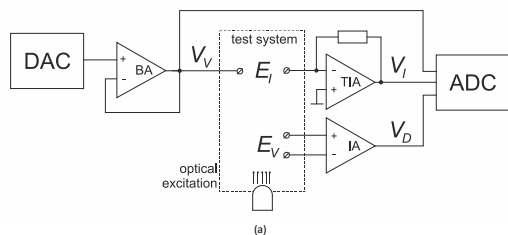


Figure 1: Experimental system with EIS MU3.4. **(a)** Structure of one measurement channel, DAC,ADC – analog/digital converters, TIA – transimpedance amplifier, BA,IA – signal amplifiers, V_I , V_V , V_D – excitation and response signals, E_I , E_V – current and potential electrodes, see (CYBRES, 2018b) for more detail; **(b)** Five differential measurement systems operating in parallel with optical 470/940nm and electrical excitations of water samples.

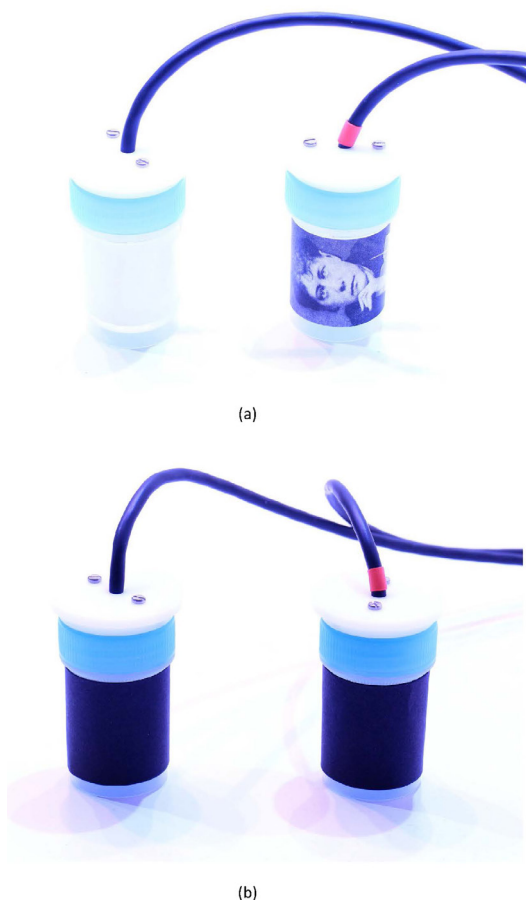


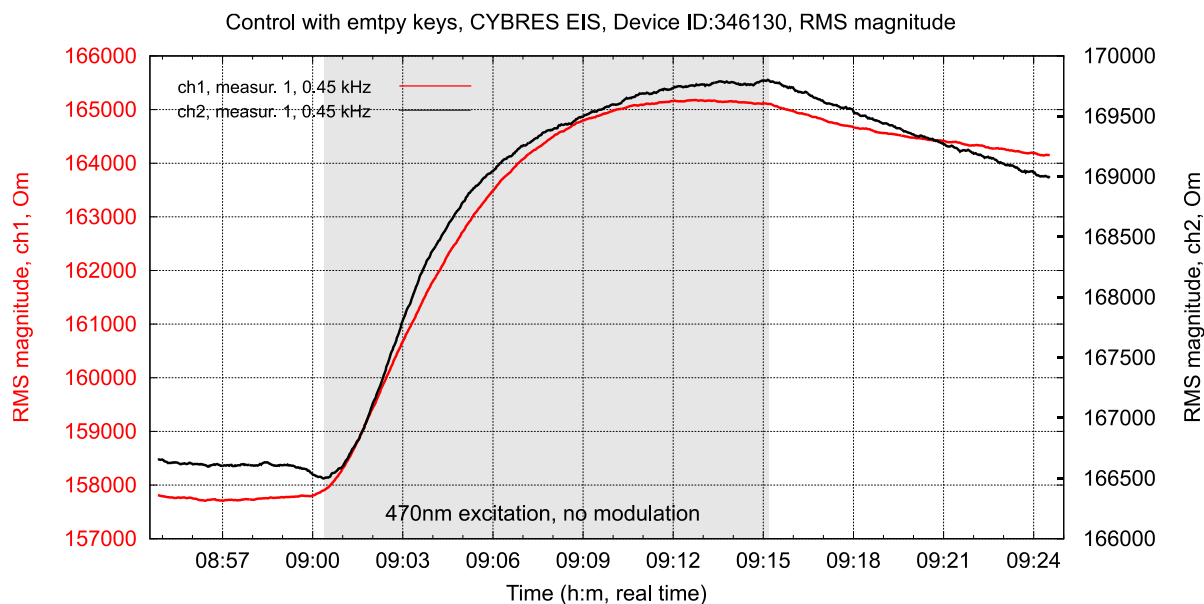
Figure 2: **(a)** Image of Helena Blavatsky on the first channel, printed on the outer side of the 'key' (to keep equal reflective inner surface of both 'keys'); **(b)** Black matte cylinders inserted over 'keys' to remove the influence of reflecting surface on measurement results.

cylinders, see Fig. 2(a,b). Several attempts with 8 EIS devices have been performed with keys from Fig. 8(c,f) to verify that % of black color on keys does not define the final result, see Sec. 4.

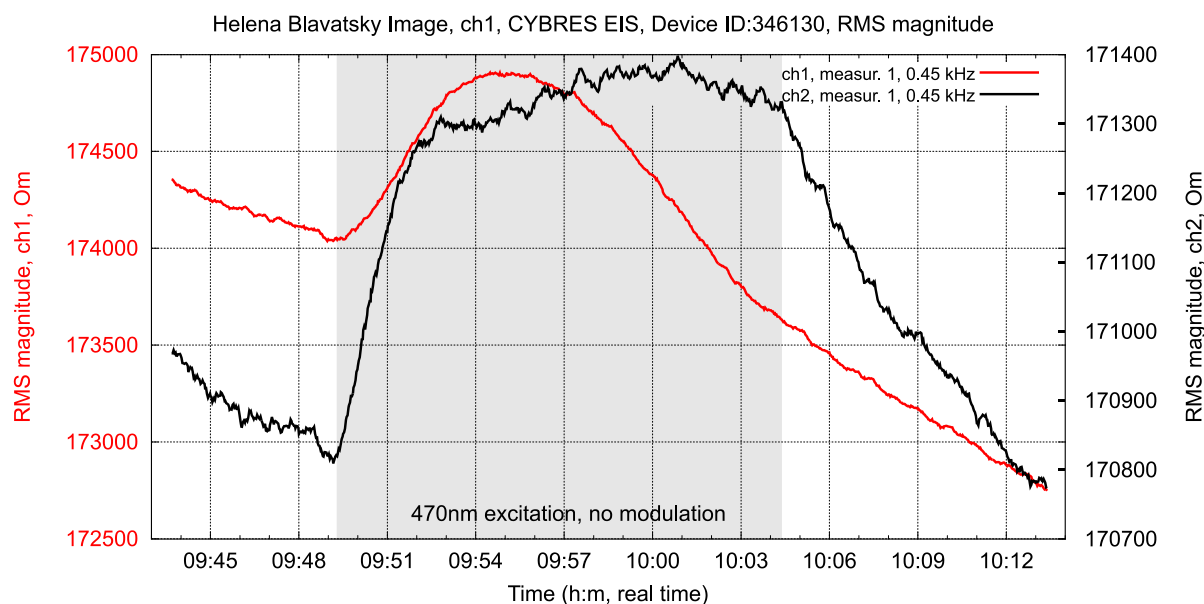
Statistical data processing. EIS dynamics of both channels, the temperature of liquids and the second statistical moments were analysed during measurements, see Figs. 5 and 6. Calculation of statistical moments is described in (CYBRES, 2018a) and follows algorithms proposed in (Press *et al.*, 1992). In short, the variation (second moment), skewness (third moment) and kurtosis (fourth moment) in a moving window of 500 or 1000 values, constantly sampled by the device, are calculated. To stabilize the statistical deviations when filling the buffer, a 'split plot' is used, which starts calculations 1 minute after the start of measurements. Readings of channel 1 are divided by channel 2 and set to zero for the same dynamics of both channels, and are displayed as bar charts. The more different is the dynamics of both channels, the higher are the bar graph values. Statistical moments are calculated independently for impedance, correlation, phase and temperature – thus a vector of 12 parameters is obtained that characterizes the state of remote object. The value of 'total score' averages the values of other parameters. Fig. 5 shows a statistical analysis of EIS dynamics from Fig. 4 by this method. To obtain a numerical result by using the statistical method, the measurement period was divided into two parts, details of this procedure and the option 'split plot' can be found in (CYBRES, 2018a). Such a time-differential approach allows removing the trend variation of both channels and so that to focus only on differences of EIS dynamics between channels. Denoting the 'total score' value of the control measurement as σ , the result of experimental measurement is considered significant at $>3\sigma$.

Protocol. Experiments on non-local signal transmission showed the greatest efficiency when using a transmission 'window' of 25-30 minutes. The signal was detected inside such a 'window' and immediately after it, i.e. the receiver's response occurred when the non-local transmitter was turned on or off. The monitoring system follows the same methodology. The duration of excitation is 25 minutes. The EIS dynamics was recorded 5 minutes before excitation and 10 minutes after it, i.e. the measurement protocol is 5-25-10 repeated each 60 minutes. After initial measurements with 5-25-10, 0-30-0, 0-20-10, the final protocol was set





(a)



(b)

Figure 3: **(a)** Control measurement with 'empty keys' – both EIS channels follow each other; **(b)** Measurement 'Helena Blavatsky key' – 'empty key' as shown in Fig. 2(a), differences in EIS dynamics are well visible.

to 0-25-5 or 0-20-5 repeated each 30 minutes. The DA script implements an automatic execution of protocols (CYBRES, 2018b). Each experiment began with a control measurement with two empty keys, which was repeated until a 'zero level' of dynamics was demonstrated (as a rule, one measurement), after that the key was replaced in one channel and experimental measurements were performed. In each new measurement cycle only fresh water was used.

Impact of temperature. Temperature dynamics of both liquids behaves slightly different.

Reasons are different initial conditions as well as variations of setups, and, as assumed, non-local processes (this assumption underlies the thermodynamics assessment metrics, see Sec. 4). Control measurements demonstrate temperature variations between channels of 0.05C–0.08C, see Fig. 6, however contribution of temperature dynamics to overall statistical result is negligible.

Reproducibility and reliability. During experiments, two effects were noted, which also occurred with non-local communication systems and



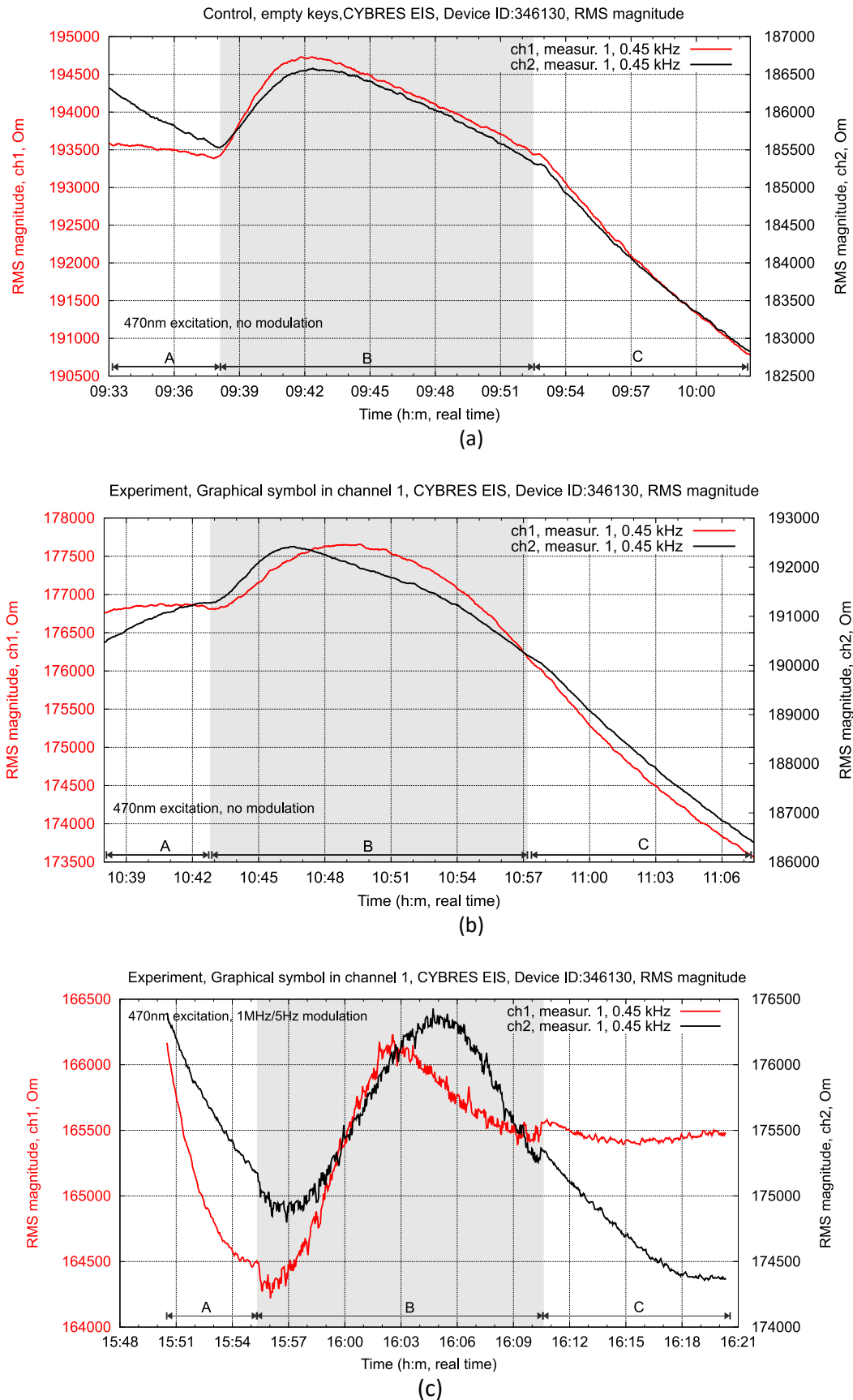


Figure 4: **(a)** Control measurement, empty keys, 470nm optical excitation without modulation, A-B-C protocol (time before excitation, excitation and after excitation) 5-15-10 minutes, EIS frequency 450Hz; **(b)** An example of different EIS dynamics, the channel 1 has the symbolic object from Fig. 7(f); **(c)** Measurement as in (c), optical excitation with modulation 1MHz/5Hz.



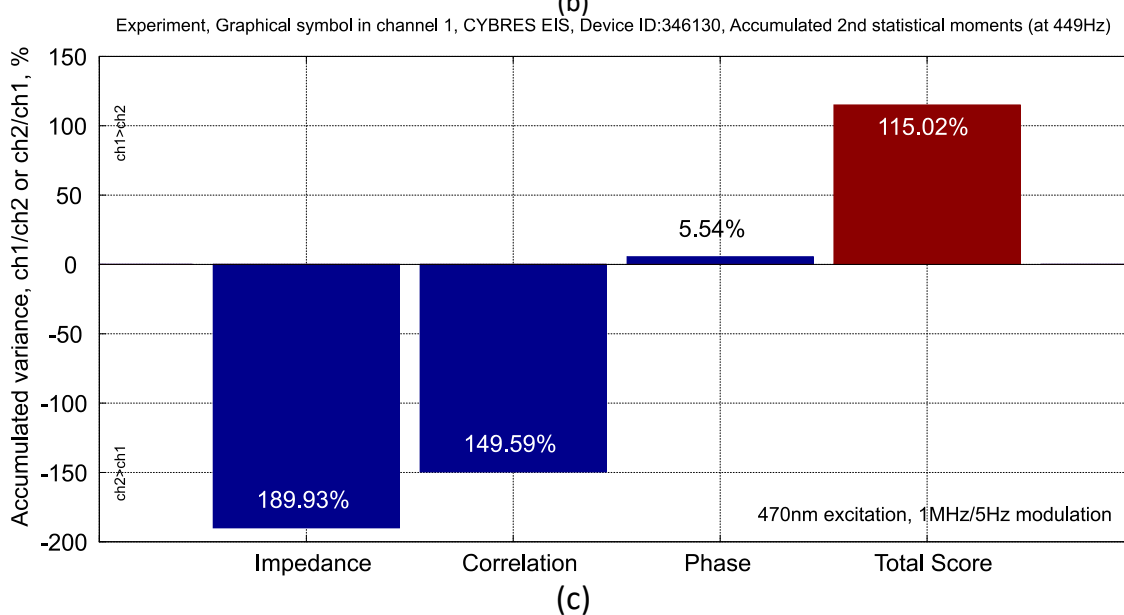
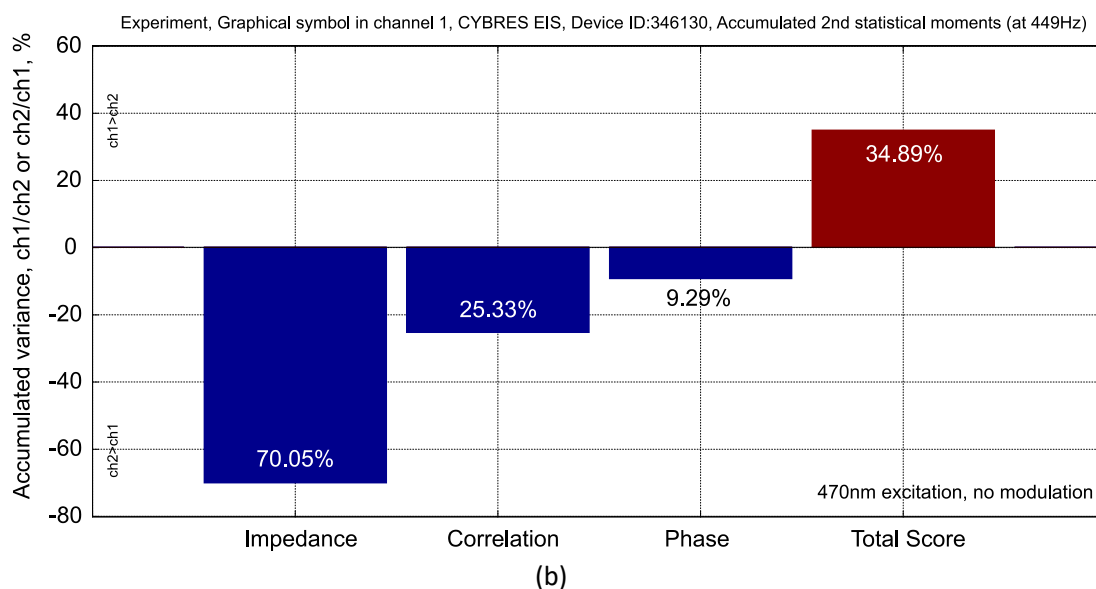
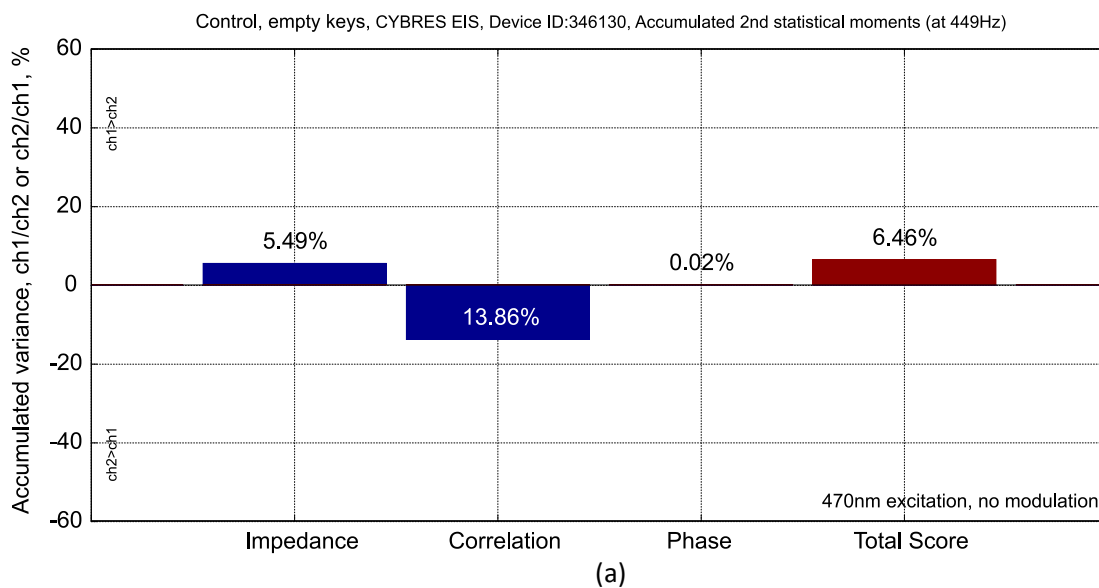


Figure 5: (a,b,c) Statistical analysis of graphs from Fig. 4(a,b,c) with bar charts, from the protocol A-B-C only the region C is analyzed.



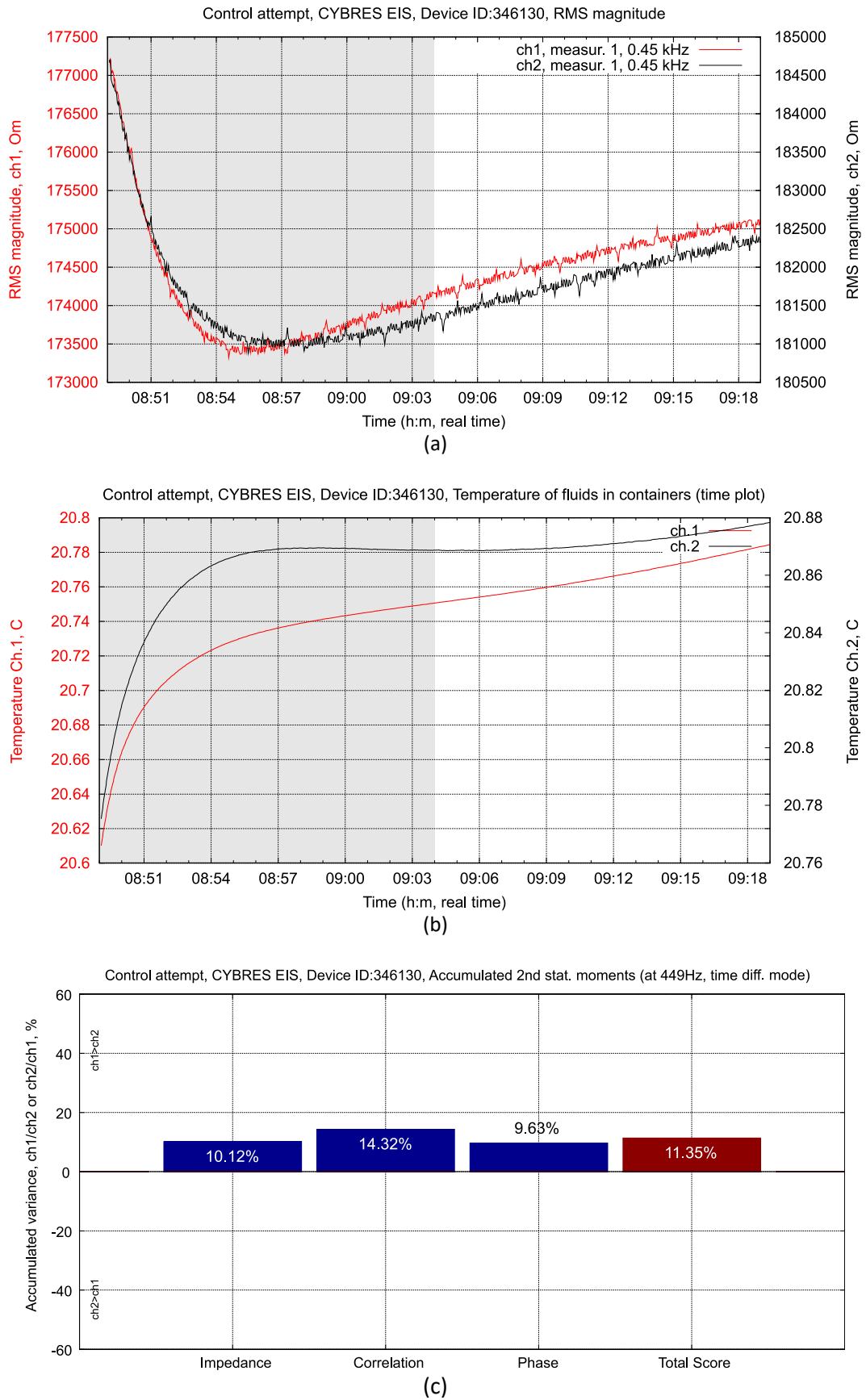


Figure 6: An example of control measurements with empty 'keys', protocol 0-30-0. **(a)** EIS dynamics of both channels; **(b)** Temperature of both channels with liquids; **(c)** The second statistical moments.



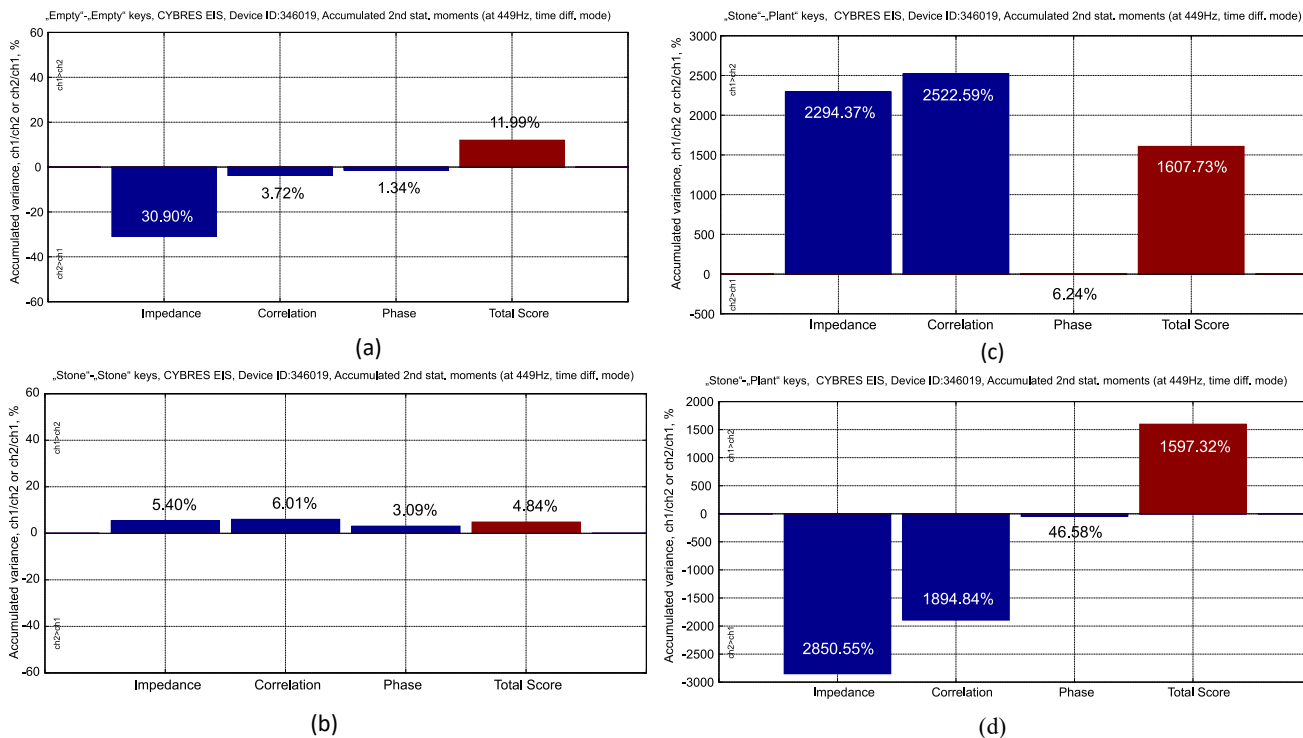


Figure 7: Example of calibration measurements with objects from Fig. 8(a,b), protocol 0-60-0. **(a)** Control measurements with empty keys; **(b)** Calibration measurements with keys 'stone' - 'stone'; **(c,d)** Two iterative calibration measurements with 'plant' - 'stone' keys on the same EIS device.

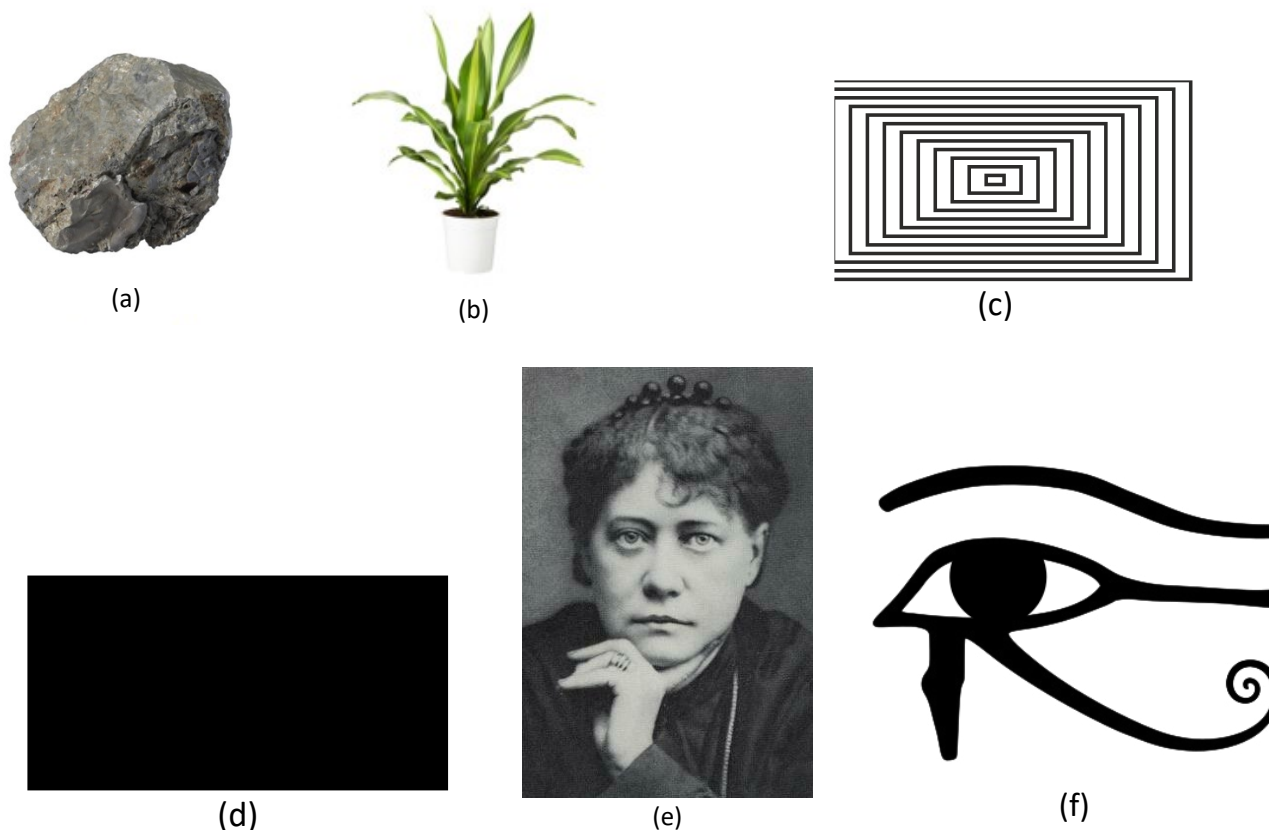


Figure 8: Examples of various objects (keys) for monitoring. Calibration objects – **(a)** Stone; **(b)** Plant; **(c,d)** Geometrical patterns; **(e)** Photo of Helena Blavatsky, from en.wikipedia.org/wiki/HelenaBlavatsky, **(f)** 'Eye of Horus', Ancient Egyptian symbol.

are described in literature. Firstly, the measuring system at some points did not work with distant objects. For example, the system of non-local communication (Kernbach, 2013a) demonstrated about 70%–80% of operability (one from four devices was 'blocked' in most cases). Remote monitoring system has a similar behaviour, e.g. one from 8 EIS devices has anomalously high values (see discussion in Sec. 4). This effect characterizes the 'reproducibility' parameter, which can be improved by using multiple EIS devices working in parallel (however multiple EIS meters can interact with each other through a common measured object).

Secondly, repeated measurements of the same object show a gradual decrease of readings. On the one hand this effect is related to wave-like EIS dynamics, see Figs. 11, 18 and corresponding discussions. On the other hand, this seems to be a property of non-local channel. The parameter 'reliability' characterizes this effect and limits the system by 3-5 consecutive measurements. Several methods to avoid this effect were tested – using only new keys, restarting the system with a new water, etc.

Single-Device Measurements

Single-device measurements represent the simplest system of distant monitoring without complex assessment metrics. Results are calculated as $\sigma = e_1 / c_1$, where e_1, c_1 are single control and experimental readings of 'total score', see Table 2.

Control and calibration measurements. In the control experiments, two white strips (empty 'keys') were placed on containers. An example of the EIS dynamics is shown in Fig. 6, some repeated measurements are summarized in Table 1. Calibration experiments were conducted with objects of different nature (stone and plant), see Fig. 8(a,b), the results of these measurements are shown in Fig. 7 and demonstrate a significant difference of EIS dynamics between the 'stone' and 'plant' objects.

Test measurements. Images for test experiments are selected randomly and included objects of different categories – various geometric shapes and symbols, plants, historical photographs of various people, infoceticals and self-diagnostics, geopathic zones, see Fig. 8. Protocols 0-30-0, 5-25-15, 0-20-10 and 5-15-10 were tested. Up to three repeated measurements of the same object were carried out. The system was also used for self-diagnosis of volunteers. In the first three attempts they were informed about beginning of measurements,

in the three subsequent ones – not. Subjective observations of own psychophysical state were recorded during and after the tests. In the final three attempts, the volunteers had to determine the begin of measurements. Experiments were terminated if significant psycho-physical abnormalities were reported. Some results of these measurements are collected in Table 2.

Long-term background measurements, e.g. more than 5-7 consecutive measurements, have the effect of measuring environmental variations. They are superimposed on the measurement process and make it impossible to separate a 'useful signal' from the background (i.e. entangled objects should be measured in a short time frame). However, environmental variations are interesting events, which are usually attributed to global variations of 'information field', 'field of consciousness', 'the noosphere', 'external Qi', etc. (Nelson *et al.*, 1995), (Nelson *et al.*, 1998), (Dulnev and Ipatov, 1998), (Yan *et al.*, 1999), (Qian *et al.*, 1994) (Peng and Kernbach, 2018). EIS devices can be used for both the measurements of external cosmo-biological events as well as for detecting intrinsic noospheric events. The single-channel and differential methods can be applied as described in (Kernbach, 2017b). For example, Fig. 9 shows detections of 'morning spikes', which occur at 5:00–7:00 every day, and as supposed have a global nature. In this case, the probabilistic nature of obtained data and uncertainty of 'global event' should also be taken into account.

4 Feature Matching Measurements with 8 and 16 Devices in Parallel

Differential measurement method in EIS devices allows using two keys: one channel has the object key, the second channel – empty key. In this case, double differential measurements 'empty'–'empty' keys and 'empty'–'object' keys is performed, which allows detecting anomalies of EIS dynamics introduced by a remote object. However, the second channel can contain certain 'feature keys' for 'feature'–'object' measurements. This kind of 'key'-to-'key' interactions has been already tested e.g. with pathogen fungi, plant seedlings and pepper seeds (Maslobrod *et al.*, 2014a), (Maslobrod *et al.*, 2014b), (Kernbach, 2015). The working hypothesis is that such measurements reflect distant interactions between two remote objects, in particular between feature and object, and demonstrate high values if feature and object 'match' each other.



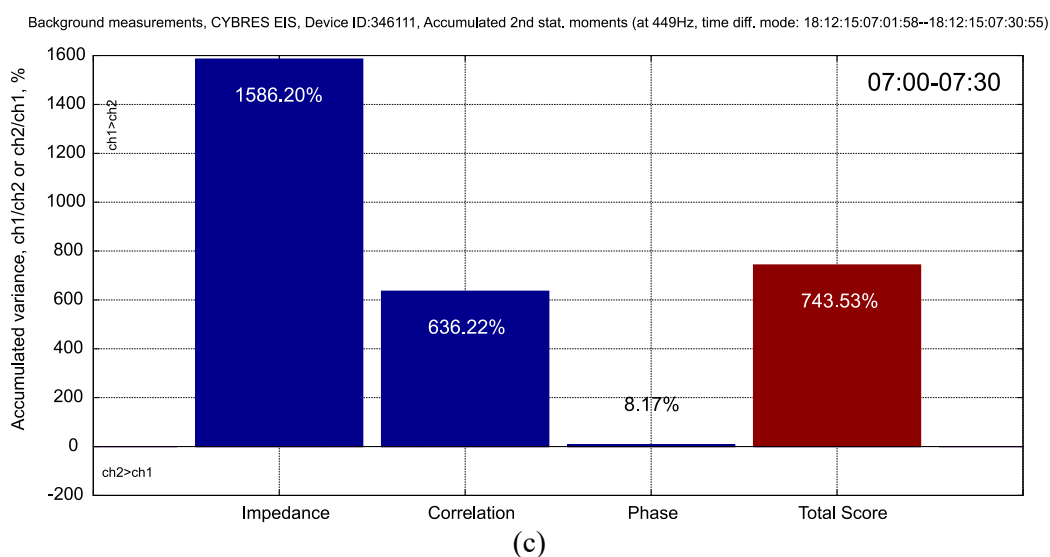
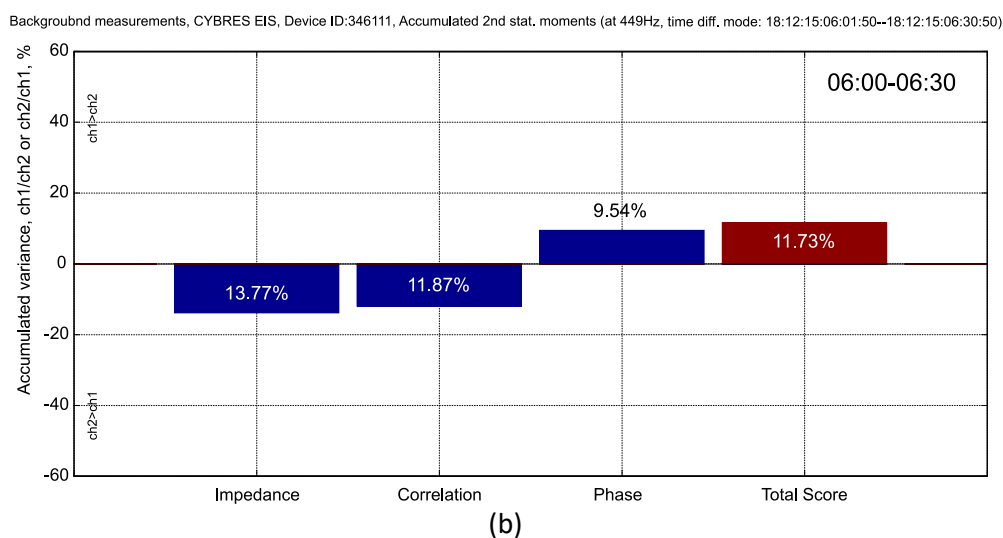
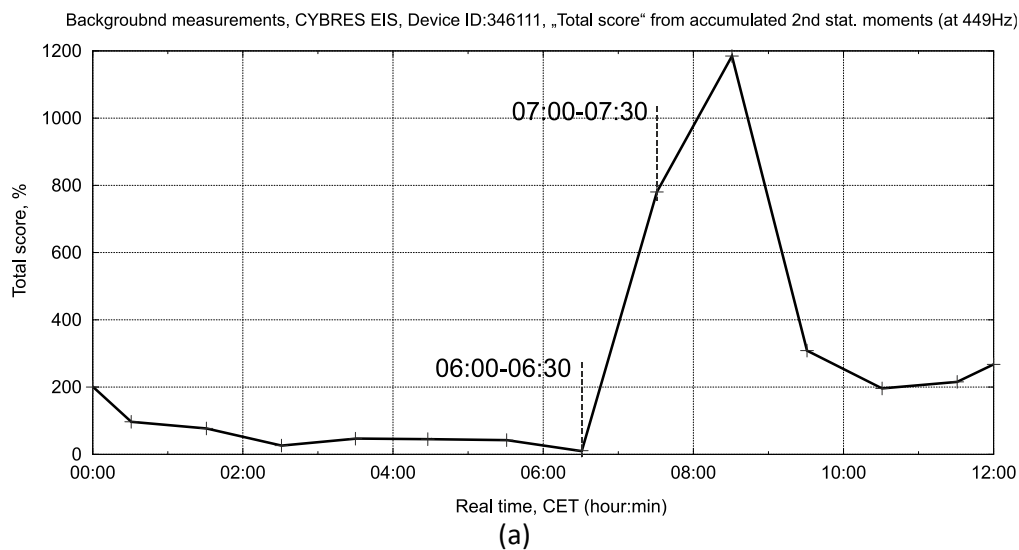


Figure 9: An example of the 'morning spike' in one of 8 EIS devices operating in parallel. Protocol 0-25-5 with optical excitation without modulation, automatically executed every hour (30 minutes measurement, 30 minutes pause) with 'empty keys'. **(a)** Interval of 12 hours of the 'total score' and **(b-c)** two examples before the 'morning spike' and after it. All EIS devices show a similar behaviour at 5:00–7:00 every day (taking into account the variation of signal with different electrodes).



Such a feature matching can be performed by several devices in parallel. Features/properties keys form a 'query byte', which, after measurement, generate a 'response byte', see Fig. 10. Measurement results can be represented in analog form as σ_i (i.e. interpreted as 'activity of interaction') or in digital form as 'matched'/'not matched' with probability of being 'true' or 'false'.

Assessment of results with σ_{\max} metric can be based on 'control to experiment' ratio as discussed earlier. For instance, Fig. 11 shows 7 consecutive measurements of 'empty'-'empty' keys and 'empty'-'symbol Fig.8(f)' keys on the same device performed two days at approximately the same time.

The assessment based on the first experimental e_1 and first control c_1 values is about $\frac{c_1}{e_1} = 10\sigma$ ($c_1 = 6.5\%$ to $e_1 = 70.4\%$ in absolute value), which repeats the data from Table 2 and confirms the method of '1 control measurement'-'1 experimental experiment' from the previous section.

The main observation is that channels with 'active key' have a wave-like perturbation in a few first measurements, whereas channels with 'passive keys' have initially a 'flat' dynamics. Denoting the absolute value of a single measurement as X_i , the following expression

$$\sigma_{\max} = x_i / \max(x_1, x_2, x_3) \quad (1)$$

provides the average value $\sigma_{\max}^{\text{control}} = 0.22$ (0.09, 0.33, 0.25) and $\sigma_{\max}^{\text{experiment}} = 0.58$ (1, 0.54, 0.21) for three first control and experimental measurements from Fig. 11. The expression (1) is denoted as σ_{\max} metric for assessing results. On the one hand, σ_{\max} demonstrates the strongest result. On the other hand, it also reflects ionic/temperature/'memory effect' anomalies during the first measurements, and has a high variation. Thus, in practical examples the parameter 'skip' is introduced, which at skip=1 starts calculation from the second value, at skip=2 from the third value and so on (to determine the begin of a 'wave').

The reason of anomalously high or low σ_i that appear randomly in some devices is a slow wave-like EIS dynamics, see Fig.11, with interchanging positive and negative phases. Depending on time when the iterative measurement is performed, it can catch only growing or only relaxing state of EIS dynamics and will result in anomalous σ_i . Increasing time between iterative measurements or changing the protocol does not resolve this issue. Phase dynamics

and appearance of anomalous σ_i are caused by local as well as non-local reasons and represent certain interest for analysis. They can be analysed 'as they are' or limited to minimal and maximal values

$$V_{\min} = 0.5 V_{\max} = 2.0 \quad (2)$$

Anomalous σ_i can be also viewed as a random interference (one or two bit are randomly 'false') that requires noise-resistant coding for the feature byte, as e.g. 2x4, 4x2 and 4x4 schemes (one feature is represented by several bits) as considered in examples later.

Assessment of results with σ_e metric. Another way to assess the results is based on several iterative measurements, which allow minimizing variation of σ_i . The differential amplitude is gradually increased in control measurements in Fig. 11(a), which reflects the degradation of electrochemical dynamics due to ionization of liquid. Denoting the average value of the first three measurements as e_3 and the first six measurements as e_6 , the expression

$$e_3 < e_6 : \text{control}, e_3 > e_6 : \text{experiment} \quad (3)$$

holds for control and experimental attempts on Fig. 10(b). The expression (3) reflects appearance of wave-like perturbation in a few first measurements in channels with 'active keys' and with (2) can be normalized to ± 1 as

$$\begin{aligned} -1 < \frac{e_3}{e_6} - 1 < 0 : \text{control} \\ 1 > \frac{e_3}{e_6} - 1 > 0 : \text{experiment} \end{aligned} \quad (4)$$

which is denoted as $\frac{e_3}{e_6}$ or σ_e assessment metric. The expression (4) can use different e values, e.g. e_2 and e_7 .

To verify this, we performed 19 experiments with 1216 independent measurements (each experiment has at least 8 independent 30 min measurements, each with 8 EIS devices), see Table 2. The result of $\frac{e_3}{e_6}$ (skip 1), with 8 bit averaging μ for control is 1.50 (or the 'true' measurement - 1.47), for experimental attempts - 0.98. Thus, (3) is confirmed on a large statistical data set.

Thermodynamic and relative metrics. As mentioned in Sec. 2, temperature inside fluids represents interesting measurement value, which reflects not only local but also non-local interactions. However, the metric, similar to (4), for temperature, e.g. $\frac{t_3}{t_6}$, demonstrates a uniform behaviour for all measurements that hereby confirms that temperature does not represent a significant parameter for



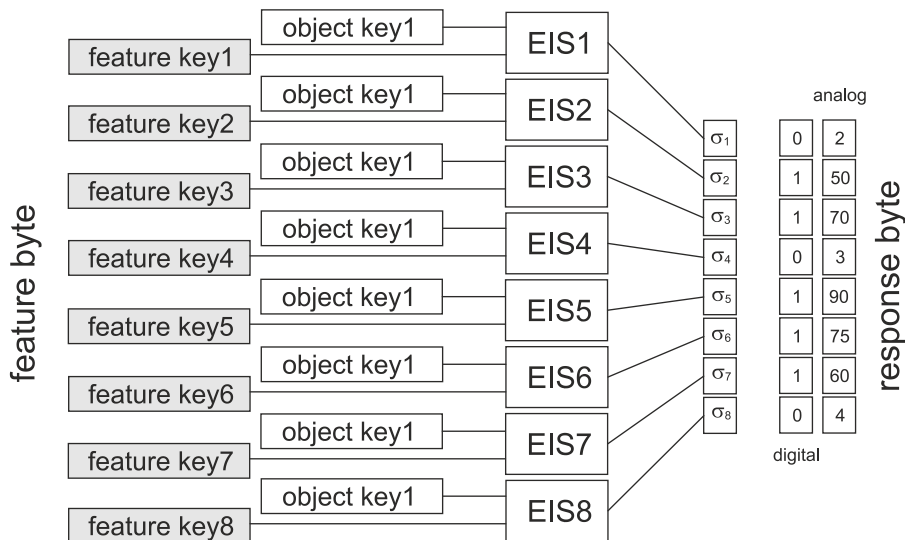


Figure 10: Graphic illustration of using EIS devices with requests and responses bytes. The resulting σ_i can be interpreted in both analog and digital forms (with probability of being 'true' or 'false');

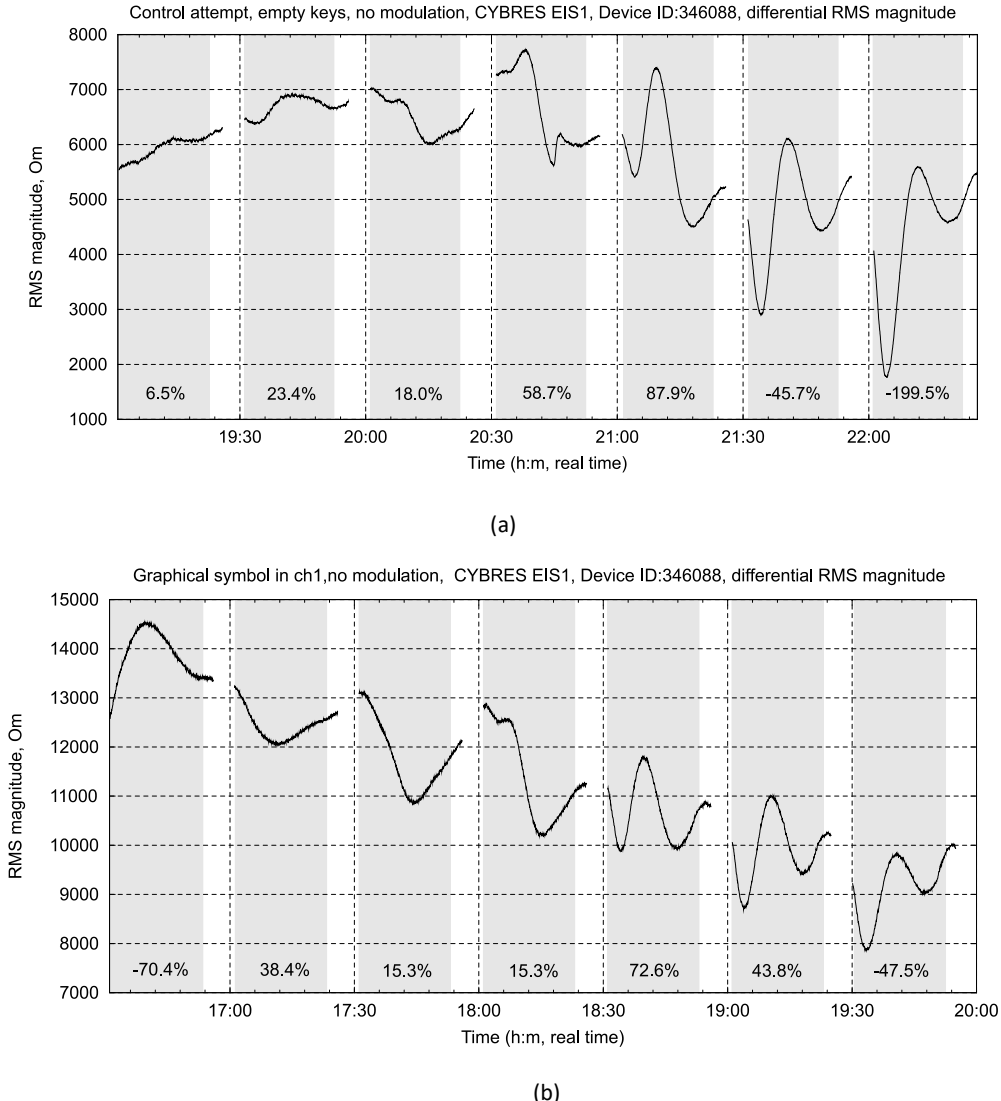


Figure 11: The differential impedance dynamics of EIS1 device with 0-20-5 protocol, the gray bar is the optical excitation, 7 consecutive measurements are shown, numbers represent statistical values of the impedance variation. **(a)** Control experiment 'empty key'-'empty key'; **(b)** Experiment 'empty key'-'symbol Fig.8(f)' in channel 1.



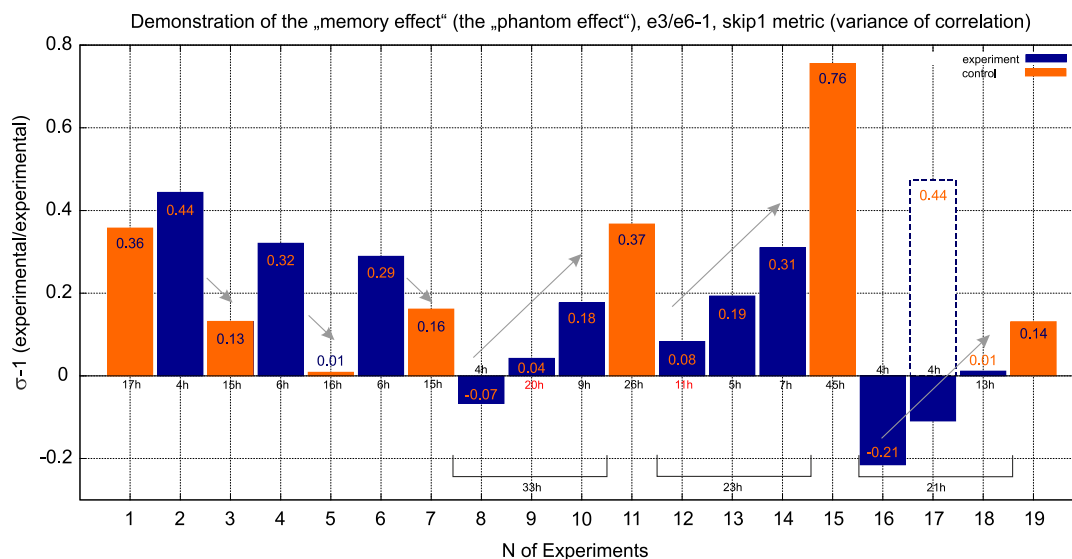


Figure 12: The 'memory effect' – influence of previous measurements on the next ones. Water is changed before each new experiment, the σ_e metric is used, duration of experiments is shown below the bars.

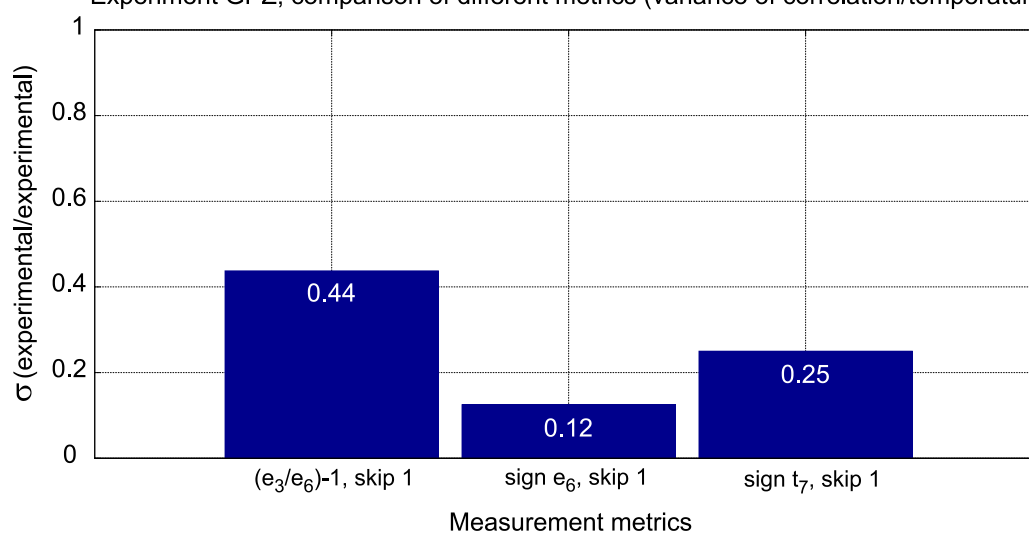


(a)



(b)

Experiment GPZ, comparison of different metrics (variance of correlation/temperature)



(c)

Figure 13: (a) Image of Rusanov's GPZ as an object' key; (b) Image of Menhir Kerloas, weight 150t, high 9.50m, Bronze Age, Brittany, France. (c) Comparison of $\sigma_e, \sigma_{\text{sign}_e}$ and σ_{sign_t} metrics for the image in Fig. 13(a).



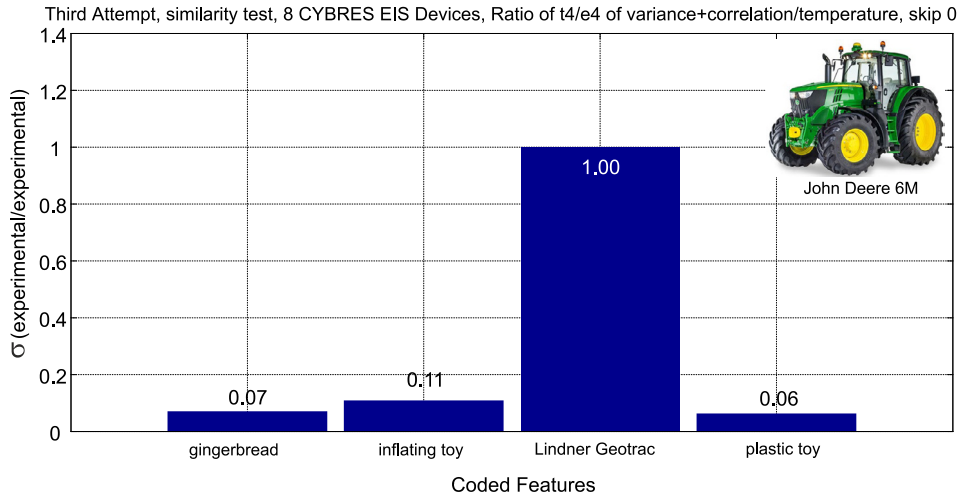


Figure 14: 4x2 feature coding with a real tractor (John Deere 6M series) as an object and four feature images (see text), shown is the last measurement from (11) with $\frac{t_4}{e_4}$ metric.

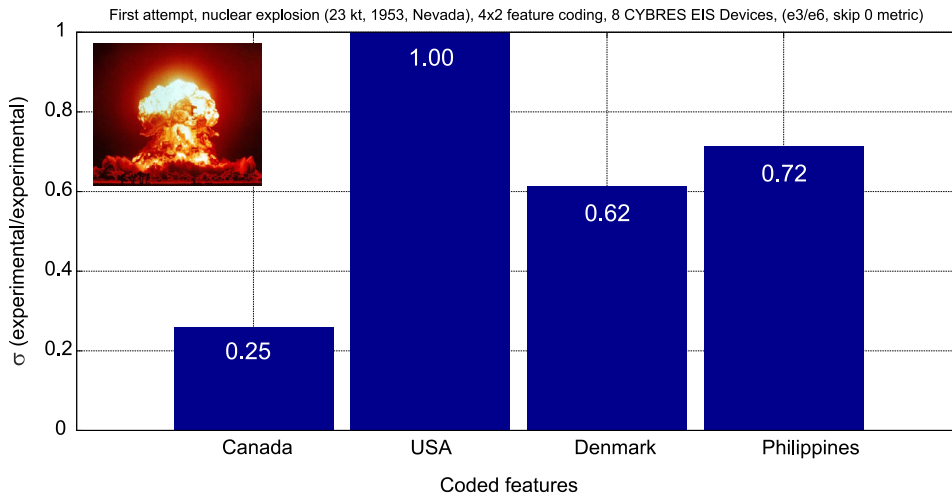


Figure 15: 4x2 feature coding with flag of Canada, USA, Denmark and Philippine, the nuclear explosion 1953 in Nevada is the object key (photo courtesy of National Nuclear Security Administration, Nevada Site Office). Shown is the first measurement from (13) with the metric $\frac{e_3}{e_6}$ skip 0, averaged by (8).

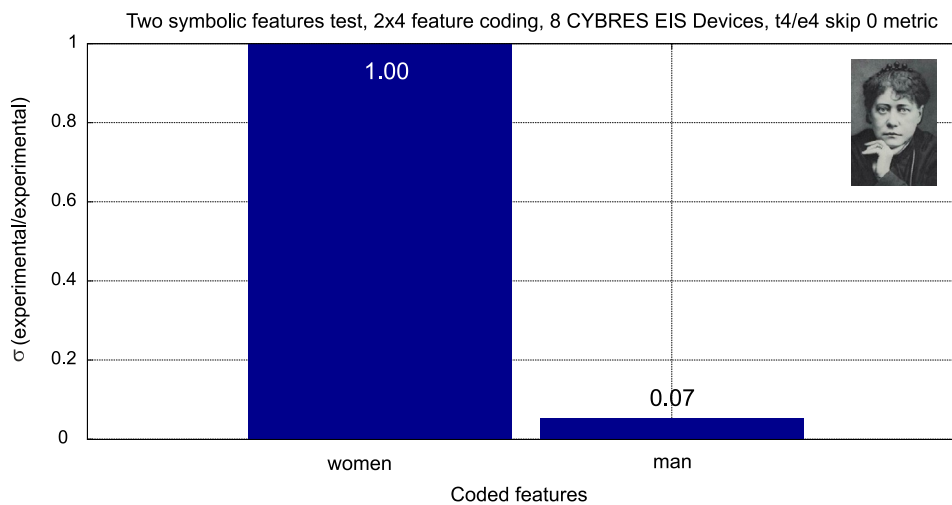


Figure 16: 2x4 feature coding with symbols A1 (male), B1 (female) (from the Gardiner list (Gardiner, 1957)) as features and the image from Fig.7(e) as the object, the metric $\frac{t_4}{e_4}$ skip 0 for coding 1 scheme is used.



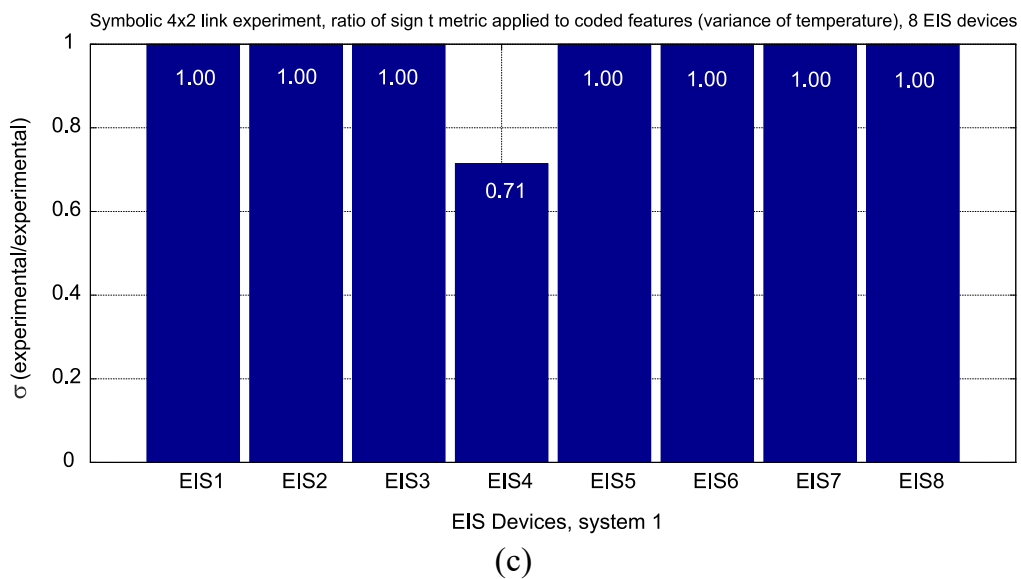
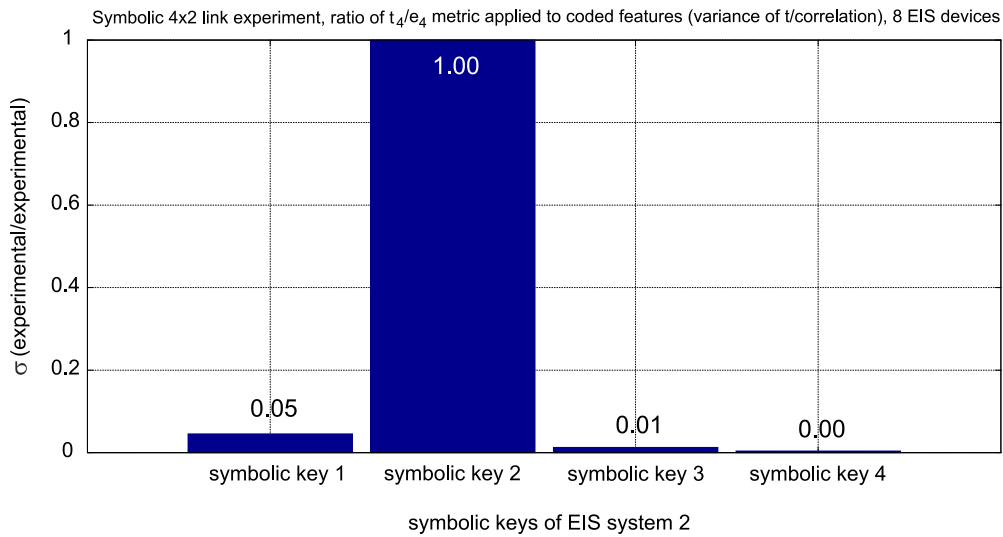
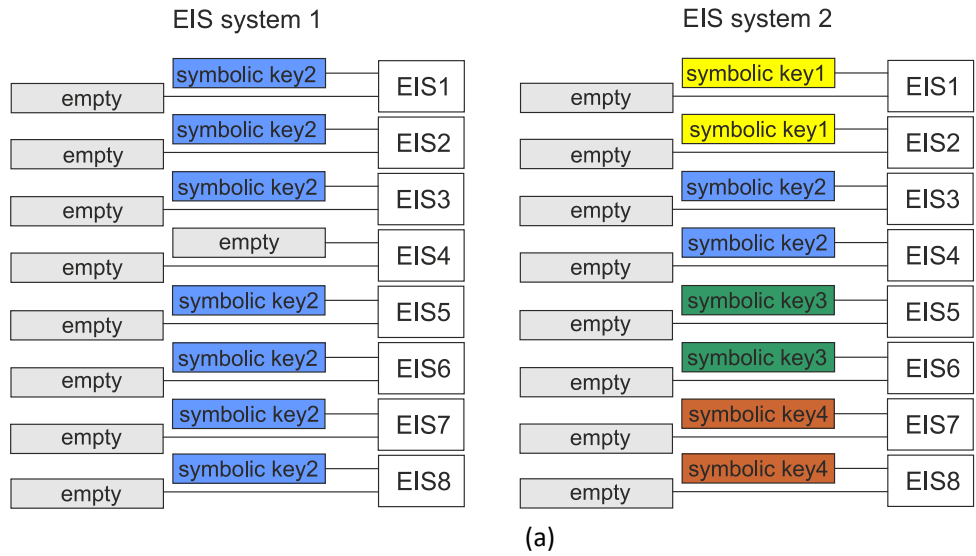


Figure 17: Experiment with cross-interactions between measurement systems. **(a)** Structure of the setup and placement of symbolic keys with 4x2 coding scheme; **(b)** One of measurements on the receiver side (the EIS system 2) with $\frac{t_4}{e_4}$ metric; **(c)** Measurement at the same time as in (b) on the transceiver side (the EIS system 1) with $\text{sign } t_7$ metric.



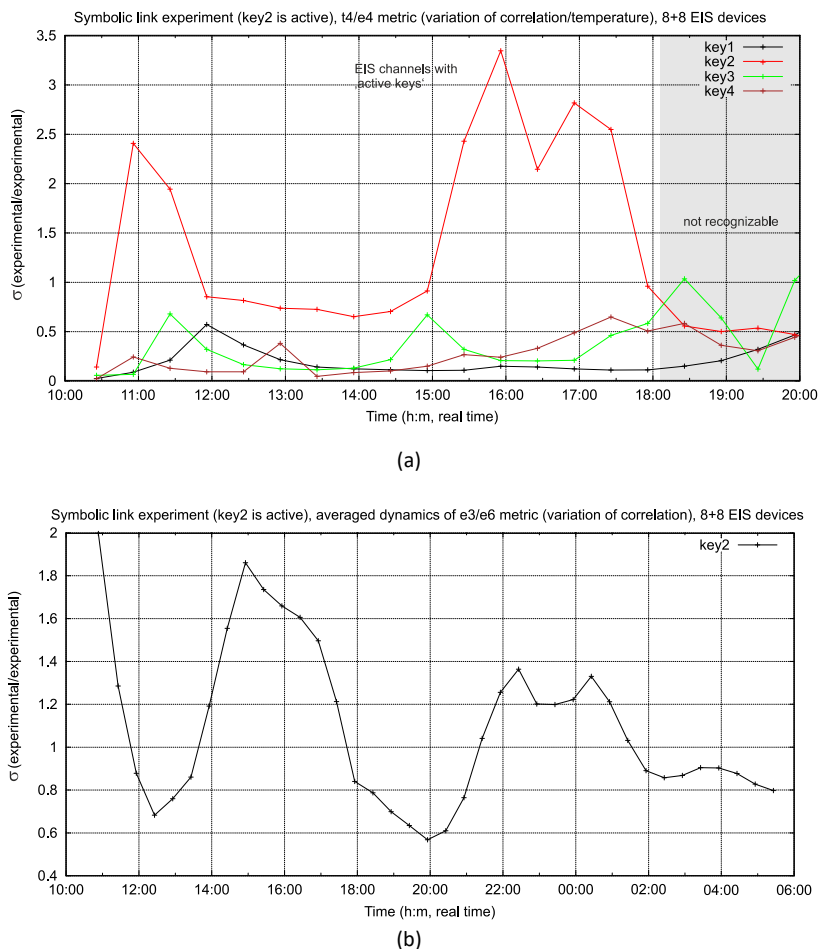


Figure 18: The receiver side, EIS system 2: dynamics of (a) channels with all four keys during 8 hours with t_4/e_4 metric; (b) channels with the 'key 2' during 20 hours with e_3/e_6 metric.

Table 1: Control measurement with a single device and 'empty keys'.

N	Impedance	Correlation	Phase	Total score	Protocol	Modulation
1	5.49	13.86	0.02	6.46	5-15-10	no
2	30.90	3.72	1.34	10.99	0-30-0	yes
3	-3.98	13.77	0.13	5.96	0-30-0	yes
4	10.12	14.32	9.63	11.35	0-30-0	yes
5	11.46	10.74	9.80	10.67	0-30-0	yes
6	14.31	14.85	7.29	12.15	0-20-10	no
7	-10.28	-10.20	11.72	10.73	0-25-5	no
8	-13.62	-14.99	4.76	11.12	0-25-5	no

Table 2: Some test measurements with a single device, values of σ are rounded, 'P1' – data from one of volunteers.

Fig.	Impedance	Correlation	Phase	Total score	σ	Protocol	Modulation
8(a)	-21.85	-27.23	5.56	20.30	2	0-30-0	yes
8(a)	40.71	42.04	11.81	29.43	2	0-25-5	no
8(c)	20.70	94.91	-43.16	52.92	4	0-30-0	yes
8(c)	-43.68	-51.03	0.87	31.86	3	0-30-0	yes
8(c)	-61.80	-61.23	2.88	41.97	4	0-20-10	no
8(d)	136.61	324.74	1.60	154.32	12	0-30-0	yes
8(d)	226.85	144.61	4.66	125.34	10	0-15-10	no
8(d)	332.60	341.42	4.15	226.05	18	0-25-10	yes
P1	219.56	239.62	18.18	159.12	11	0-30-0	yes
P1	123.61	160.68	-6.34	96.88	9	0-30-0	yes
P1	-59.74	-124.79	-96.73	93.75	9	0-30-0	yes



differential measurements. From all tested metrics, two following ones

$$\sigma_{t_i} = t_i / e_i, \quad (5)$$

$$\sigma_{\text{sign } t_i} = \text{sign } t_i = \frac{1}{N} \sum_{i=1}^N (|t_i| / t_i) \quad (6)$$

demonstrated a significant difference between control and experimental measurements. Similar dynamics possesses also

$$\sigma_{\text{sign } e_i} = \text{sign } e_i = \frac{1}{N} \sum_{i=1}^N (|\sigma_i| / \sigma_i) \quad (7)$$

metric. Both $\sigma_{\text{sign } e_i}$ and $\sigma_{\text{sign } t_i}$ have a maximal value of ± 1 . Control attempts demonstrate $\sigma_{\text{sign } e_i} \approx 0$ and $\sigma_{\text{sign } t_i} \approx 0$, which means a similar number of sign variations between channels. Experimental attempts have a symmetry break for $\sigma_{\text{sign } e_i}$ and $\sigma_{\text{sign } t_i}$ metrics, see Table 3, which can be used for assessing the results. The σ_e and σ_t metrics reflect different characteristics of EIS dynamics - σ_t indicates maximal values and is more suitable for mutually exclusive features, whereas σ_e points to wave-like dynamics and to complementary features.

Since σ_{t_i} metric (e.g. $\frac{t_i}{e_i}$) is not normalized to ± 1 , the normalization is introduced by

$$\sigma_{t_{\text{max}}} = \sigma_{t_i} / \max(\sigma_{t_i}) \quad (8)$$

which represents a histogram-like form, where maximal value is equal to 1 (or to 100%) and all other values are < 1 , see e.g. Fig. 14. This relative metric is stable to variations of common factors influencing all channels, such as the 'memory effect' or environmental fluctuations. The expression (8) can be used also for a histogram representation of other metrics.

Probabilistic aspect of measurements. As mentioned earlier, the EIS output can be considered as 'true' or 'false' in regard to some requested fact. For instance, based on Table 3, the $\frac{e_3}{e_6} = p_1 = 1.50$ can be set for being 'true' in regard to the statement 'symbol Fig.8(f) is active' and $\frac{e_3}{e_6} = p_0 = 0.98$ as 'false' for this statement. Since σ_i floats between p_0 and p_1 , it makes sense to present them as deviation p_i from p_0 calculated as

$$p_1 = \frac{(p_0 - \alpha_i)}{p_0} \quad (9)$$

where α represents some physical limitations in the system. In a simple case, $p_0 = 1$ and (9) represents the metric (4) with minimal V_{min} and maximal V_{max} as (2) and $\alpha = 1$. An averaged p is calculated as

$$p = 1/n \sum_{i=1}^n p_i, \quad (10)$$

where n is a number of equal feature bits (in case of empty feature byte $n=8$). The expression (9) reflects the probabilistic character of p_i , and the averaged p value for can viewed as the probability of being 'true' for the given measurement. The expression (10) can be applied for estimating the probability of 'true' for multiple iterative measurements with (8) metric and '= 1' and '≠ 1' outputs.

The approach (9), (10) requires repetitive control measurements for calibrating the values of p_0 and α . This is reasonable taking into account metal-to-water ions transfer in electrodes and environmental changes. Too high p values of control attempts (or too low values of experimental attempts) indicate environmental variations/'memory effect' and should be removed from consideration as 'not reliable'.

Table 3: Different metrics for assessing results, control attempts are with 'empty'-'empty' keys, variance of correlation/temperature are measured with 8 EIS devices, μ - mean values, skip 1 is applied to all metrics.

N	$\frac{e_3}{e_6}$	sign e_6	sign t_7	N	$\frac{e_3}{e_6}$	sign e_6	sign t_7
Control, empty keys				Experiment, Fig.8(f)			
1	0.95	0.16	0.32	11	1.43	0.50	0.21
2	1.08	0.08	0.07	12	1.55	0.16	0.60
3	1.08	0.04	0.35	13	1.49	0.16	0.42
4	0.96	0.08	0.17	μ	1.50	0.27	0.41
5	0.99	0.16	0.17	'False' test, Fig.8(c,d)			
6	0.97	0.00	0.25	14	1.12	0.20	0.10
7	1.05	0.04	0.00	15	1.07	0.04	0.21
8	0.85	0.08	0.17	16	0.90	0.12	0.35
9	0.89	0.04	0.07	μ	1.03	0.12	0.22
10	1.00	0.04	0.07	'True' test			
μ	0.98	0.07	0.17	17	1.45	0.08	0.43
				18	1.58	0.21	0.32
				19	1.39	0.00	0.32
				μ	1.47	0.09	0.35



The memory effect manifests in influencing current measurement by a few previously performed experiments. Physical nature of this effect is unclear, it is also known as the 'phantom effect' (Kernbach and Zhigalov, 2013), (Persinger and Dotta, 2011). Fig. 12 demonstrates 19 experiments (3536 measurements inside and outside of the $\frac{e_3}{e_6}$ metric, each of 30 min duration, following each other). Blue bars show experiments with active keys, the orange ones – with empty keys (control attempts). According to (4), the orange bars should be lower than blue ones. This holds for experimental attempts with one iteration. Attempts with three iterations demonstrate increasing values between attempts and the controls are higher than the experiments (with significant drops of the next experimental attempts). This effect has several consequences: 1) absolute value of the attempt contains the memory effect whose influence should be separately estimated; 2) 'relaxing' control attempts (always with the same, e.g. empty, keys) should be performed between experiments; relaxation can be performed by switching off the system; 3) iterative experimental attempts provide better results however require increasing the number of 'relaxing' attempts. Generally, the relative metrics like (8) are more stable to the memory effect than the absolute ones; their usage is more preferable.

Failure of the feature matching approach should be differentiated from negative results. Criteria for assessing the result as failure are inconsistencies, e.g. similar probabilities for mutually exclusive features or low σ_i values for control and following experimental attempts. Unclear, too general or context-dependent symbolic keys (e.g. simple geometric shapes such as triangles, cycles etc.) produce methodological failures, such keys are not suitable as feature bytes. Technical failures occur due to different propagation of perturbation in phase space of all EIS devices (the 'skip' parameters), see Fig. 11. The wrong selection of the 'skip' parameters among EIS devices leads to inconsistency of $\frac{e_2}{e_5}, \frac{e_3}{e_6}$ and $\frac{e_4}{e_7}$ evaluation criteria and finally to wrong overall probability values. From all performed experiments, about 1/5-1/4 of results can be assessed as technical failures.

Test Measurements

The 'false' and 'true' test measurements. A priori known 'true' and 'false' test measurements are intended for calibration purposes. Examples

of objects for 'false' measurements are geometric patterns in Fig. 8(c,d) with empty feature bytes (the geometric pattern from Fig. 8(c), publicly discussed during preparatory works, was replaced by a similar pattern). Null hypothesis is that the case of 'empty'-'geometric pattern' keys should be similar to the case of 'empty'-'active object' keys. 'True' measurements are performed with the image of sun (courtesy NASA) as a key. Results are summarized in Table 3, the mean μ differs between control and experimental attempts, thus, we consider it as a rejection of the null hypothesis for the 'false' and confirmation of the 'true' measurements.

Geographic object. Tests with geographic object and empty feature keys (geographic object is a geopathic zone (GPZ) discovered on 25.05.18 by A.Rusanov in Stuttgart) shown in Fig. 13(a). Anomalous effect of this GPZ was measured earlier (see water samples on the image), here the measurement 'empty keys'-'GPZ' should provide a non-local estimation for 'GPZ is active'.

About 10 control and 10 experimental measurements with 0-20-5 protocol repeated once each hour, i.e. 160 independent attempts. As described above, the values $\sigma_e, \sigma_{sign_e}$ and σ_{sign_i} of σ_i are calculated, see Fig. 13(c). All metrics are over the control and 'false' measurements from Table 3, the activity index can be set to the $\frac{e_3}{e_6}-1$ value of 0.44 that indicates a high activity of this GPZ.

Test of 4x2 feature coding with real macro-objects is performed by selecting a real tractor (John Deere 6M series) as an object and four feature images: 1) gingerbread 'tractor', 2) inflatable toy-tractor, 3) Lindner Geotrac tractor and 4) plastic toy-tractor. Experiments are repeated three times (protocol 0-20-5 repeated once each 30 minutes, 3x10 attempts with 8 EIS devices), feature coding (each feature represented by 2 bits) and results by using $\frac{t_4}{e_4}$ metric are



(0.03 0.04	0.19 0.02	0.19 0.19	0.02 0.003)
(0.01 0.06	0.008 0.10	0.17 0.11	0.03 0.008)
(0.007 0.006	0.014 0.006	0.13 0.06	0.007 0.005)

with averaging between groups



$$\begin{pmatrix} 0.20 & 0.57 & 1.00 & 0.06 \\ 0.29 & 0.38 & 1.00 & 0.16 \\ 0.07 & 0.11 & 1.00 & 0.06 \end{pmatrix} \quad (11)$$

The last measurement is shown as a bar graph in Fig. 14.

Test of 4x2 feature coding with abstract objects can be demonstrated by using the image of nuclear explosion 1953 in Nevada and the feature byte consisting of flags of Canada, USA, Denmark and Philippine (each coded by two bits). This experiment has been performed two times (protocol 0-20-5 repeated once each 30 minutes, 2x8 attempts with 8 EIS devices), results calculated by $\frac{e_3}{e_6}$ skip 0 and skip 1 metrics for the first and second experiments are



$$\begin{pmatrix} 0.50 & 0.50 & 2.00 & 2.00 & 2.00 & 0.50 & 2.00 & 0.86 \\ 2.00 & 0.73 & 1.54 & 2.00 & 2.00 & 0.57 & 0.50 & 1.20 \end{pmatrix} \quad (12)$$

with group averaging calculated by (8)

$$\begin{pmatrix} 0.25 & 1.00 & 0.62 & 0.72 \\ 0.77 & 1.00 & 0.73 & 0.46 \end{pmatrix} \quad (13)$$

The bar graph of the first attempt is shown in Fig. 15.

2x4 feature coding with symbolic features. Symbolic objects provide sometimes a high activity index. To test this approach with symbolic features, we selected symbols A1 (male), B1 (female) from the Gardiner list (Gardiner, 1957) as features and the image from Fig.8(e) (E.Blavatsky) as an object. To increase reliability of detection, two features are coded by 4 bits each, i.e. 4 EIS devices measure 'feature 1'-'object', 4 other EIS devices measure 'feature 2'-'object'. Experiment (protocol 0-20-5, 8 iterations each 30 minutes with 8 EIS devices) was repeated two times with inverse coding of features



Results are evaluated with different metrics by using (8) (i.e maximal feature is always equal to 1) and are shown in Table 3. Since features are mutually exclusive, the maximal value represents the correct result. The metric $\frac{t_4}{e_4}$, skip 0 for coding scheme 1 is shown in Fig. 16. This measurement exemplifies the fact that the correct estimation appears in multiple metrics.

Scheme with 4x4 feature coding (4 bit resolution per feature) provides the most stable results and requires 16 EIS devices for 4 features. As a historical and ethnological example we selected the Menhir Kerloas as an object – the megalith in Brittany, France, see Fig. 13(b). According to legends, this menhir facilitates birth of children (in particular boys) and possesses healing properties. Corresponding historical question is whether the menhir was related to fertility, lunar or solar Neolithic cults. Corresponding features are coded by images of 'Cosmos', Earth, Moon and Sun on 16 devices:



bits: 1; 2; 9; 10 3; 4; 11; 12 5; 6; 13; 14 7; 8; 15; 16 which represent mutually exclusive features for the matching approach. From ethnological point of view, such four features are a 'typical mythological basic' and we are also interested in a complementary view on these features; their correlations with the menhir can point to a possible usage of this object.

This experiment was repeated 3 times and can be represented as 3x16x8 or 6x8x8 measurements – the last scheme provides better statistical properties (totally 384 measurements each of 30 min). Table 5 demonstrates averaged outcomes for each feature with a few $\frac{t_i}{e_i}$ and $\frac{e_3}{e_6}$ metrics calculated by (8) and then averaged.

The averaged activity index of this object is 0.445 calculated from 6 experiments (0.65, 0.39, 0.38, 0.61, 0.25, 0.39). Thus, the menhir is still an 'active object' with a high activity index. The $\frac{t_i}{e_i}$ metric reflects mutually exclusive features, which is the Sun and points to solar cults (with the probability of 9/12, i.e 75% of 'true'). Interesting outcomes provide $\frac{e_3}{e_6}$ metric, which reflects complementarity of features – the menhir has almost equal correlation with all four features (a bit higher value of the feature 3 (moon) can be explained by a 'full moon condition' during measurements). Complementarity metric can point to a practical usage of menhir – as a king of 'harmonization device' and explains its healing properties. As mentioned, these outcomes represent only a possible initial point for further historical and ethnological investigations.



Table 4: Different metrics for assessing results of 2x4 feature coding experiment calculated by using (8).

metric	coding 1		coding 2	
	women	man	man	women
$\frac{e_3}{e_6}$, skip 1	1.00	0.92	0.75	1.00
$ \text{sign } t_6 $, skip 1	1.00	0.40	0.54	1.00
$\frac{t_1}{e_4}$, skip 0	1.00	0.07	0.95	1.00
$\frac{t_1}{e_5}$, skip 0	1.00	0.36	0.40	1.00

Table 5: Different metrics for assessing results of 4x4 feature coding experiment with Menhir Kerloas, averaged over 6x8 measurements.

metric	coded features			
	1	2	3	4
$\frac{t_1}{e_4}$, skip 0	0.22	0.26	0.15	0.86
$\frac{t_1}{e_5}$, skip 0	0.30	0.39	0.21	0.89
$\frac{e_3}{e_6}$, skip 1	0.89	0.75	0.90	0.77
$\frac{e_3}{e_6}$, skip 0	0.82	0.81	0.91	0.81

Cross-interactions between measurement systems

Measurement systems with optical excitation interact with distant objects. In order to demonstrate this effect, we conducted 3 experiments (with duration of 9, 28 and 24 hours with 1952 separate measurements) with 2 EIS systems consisting of 8 devices each. Four different symbolic keys (random symbols printed on labels) were prepared and installed on EIS devices as shown in Fig. 17(a).

The EIS system 2 represents the 'receiver', whereas the system 1 appears as a 'transceiver', the distance between both systems was about 15 meters (two separate laboratories), the distance between water containers within one EIS system was 4-5 cm. Both systems continuously operated with 0-20-5 protocol repeated each 30 minutes. The measurement results are shown in Fig. 17(b,c), we discover a strong response in channels with the symbolic 'key 2' in the system 2. There are also anomalies in the system 1 – the thermodynamic metric $(6) \sin t_7$ demonstrated lower values in the EIS 4, which had empty keys. Correlations of temperature-based metrics with active symbolic keys represent interesting research issue pointing to changed thermodynamics conditions during non-local operations. Since the non-local signal generated a wave-like response, the dynamics of all four keys during 8 hours with $\frac{t_1}{e_4}$ metric and the dynamics of the 'key 2' during 20 hours with $\frac{e_3}{e_6}$ metric are plotted in Fig. 18(a,b).

We observe here three waves – 1-2, 5-6 and 11-12 hours after begin of experiments, channels without 'active keys' do not demonstrate such a wave dynamics (this behaviour can underlie additional assessment metric). All three experiments have a similar behaviour (the experiment 1 demonstrated only the first and second waves). These experiments clearly demonstrate that EIS systems interact during measurements and a response on non-local signal has a wave-like dynamics. Currently we cannot say whether such a dynamics is related to previously non-existing symbolic keys, generally represents a property of non-local signal transmission, or is characteristic to EIS systems with slowly degrading impedance. Repetitive experiments with already used symbolic keys (in the same setup with new water) generate only weak effects shown in Fig.18, or do not generate them at all. The scheme in Fig. 17(a) can represent multiple practical applications of this approach.

Conclusion

This paper reports about several thousands of measurements carried out with various macro-objects. Protocols 0-30-0, 5-15-10, 0-20-10, with or without modulation of optical excitation, were tested. Before each experiment, control measurements were carried out with empty keys to calibrate the system. It was found that several local and non-local factors influence the measurement result. Carefully considering the methodology and testing counter-hypotheses (e.g. reflecting surface affects the result), the expressed hypothesis about interactions between measurement fluids and distant macro-objects cannot be rejected. With proper preparation of electrodes, the activity index in the control experiments is 15-40% with single device, depending on the protocol, setup, and electrodes. Considering this value as a basic variation of σ , tests with known biological organisms, such as plants, are at $> 3\sigma$. More complex experiments with multiple devices and iterative measurements confirmed these initial results and also demonstrated a significant difference between control and experimental attempts based on the σ_e , σ_t , σ_{sign_t} , σ_{max} and $\sigma_{t_{\text{max}}}$ metrics.

Quantitative results vary in consecutively repeated measurements. The main difficulty represents the wave-like dynamics of experimental channels with interchanging positive and negative phases. The used statistic approach with fixed time intervals catches different combinations of



such phases and thus requires parametrization of $\frac{e_i}{e_i}$ and $\frac{t_i}{e_i}$ metrics. To improve this issue, it needs to redesign the evaluation approach on the level of basic signal processing algorithms. Generally, the parametrization, the mentioned issues of environmental fluctuations and the memory effect impact reproducibility and reliability, and represent a probabilistic nature of distant monitoring. The introduced p metric enables expressing the result as a probability of being 'true' about the measured result. It also requires iterative control measurements to calibrate the p_0 level.

The matching approach in this and other works demonstrated that distantly interacting 'similar' macro-objects generate a high activity index. However, this effect is not understood, neither in the basic mechanisms nor in the definition of 'similarity'. This is especially relevant for several investigated symbolic objects that also generate a high activity index. Context-dependent symbolic keys or simple geometric shapes produce negative result or methodological failures. This approach requires accumulation of larger statistics for different symbolic objects. In fact, one of purposes of this paper is to share collected so far results in the EIS community, and to stimulate replications of this work by different researchers.

The need for modulation of optical excitation remained open – in both cases, the result of $> 3\sigma$ was recorded. It can be assumed that modulation is a more invasive method of distant measurements, which gives better resolution for some objects (for example, symbols). The role of a human operator remains uncertain in this work. Current assumption is that the monitoring system is too complex to be purposefully influenced by operator's (un)consciousness. Since this system is commercially available, replications of this technique will determine the role of an operator.

In terms of results, firstly, the distant monitoring even at the $\approx 3\sigma$ level is useful when no other sources of information is available. The technique shown in Fig. 10 allows testing several hypotheses about distant macro-objects. Taking into account probabilistic nature of information, and a need of its independent verification, the distant monitoring can be a part of more complex system for working with remote biological, geographic, physical, or symbolic objects. Secondly, when monitoring human persons, volunteers reported about different neurological manifestations – changes in perception,

consciousness and sleep patterns, however due to ethical issues no systematic research in this direction has been conducted. It can be assumed that the use of this and similar techniques can raise ethical questions, as already discussed in (Kernbach, 2017a).

Acknowledgement

This work is partially supported by the FET Innovation Launchpad Project: 'E-SPECTR: Excitation Spectroscopy Sensor', grant No: 800860 and the quantum research and innovation program of CYBRES GmbH.

References

- Akimov A, Ochatriin A, Finogeev V. Visualization, processing and analysis of torsion information on space images (rus). Horizons of science and technology of the XXI century: works. T.1, Intern. In-t theory and applied Physics RAEN – M.: Folium, 2000; pp: 101-128.
- Akimov A, Tarasenko V, Tolmachev S. Torsion communication – new system for telecommunication (rus). Electrocommunication (Electrosvjz) 2001; (5).
- Anders J and Vedral V. Macroscopic entanglement and phase transitions. Open Systems & Information Dynamics 2007; 14: 1-16.
- Cardeña E. A call for an open, informed study of all aspects of consciousness. Front. Hum. Neurosci 2014; 8(17): 1-4.
- CYBRES. Application Note 20. Analysis of electrochemical noise for detection of non-chemical treatment of fluids. Cybertronica Research. 2018a
- CYBRES. EIS Differential Impedance Spectrometer for electrochemical and electrophysiological analysis of fluids and organic tissues. User Manual. Cybertronica Research. 2018b.
- Dulnev G and Ipatov A. Investigation of energo-information exchange: experimental results (rus). GITMO, S-Petersburg. 1998.
- Dunne B, Nelson R, Jahn R. Operater-related anomalies in a random mechanical cascade. J. of Scientific Exploration 1988; 2(2): 155-179.
- Gardiner A. Egyptian Grammar. Being an Introduction to the Study of Hieroglyphs. Oxford University Press, Oxford. 1957.
- Ghirardi G, Rimini A, Weber, T. Unified dynamics for microscopic and macroscopic systems. Physical review D: Particles and fields 1986; 34:470-491.
- Glowatzki T and Häder P. Einblick in die Erde: Neues Remote-Sensing-Verfahren revolutioniert die Wasser- und Ressourcensuche, Berlin – Raum&Zeit. 193/2015 (GSS - GeoScan Technology https://www.raum-und-zeit.com/cms/upload/Consulting/Geoscan_komplett_2.pdf)
- Gorbatych V, Saveliev G, Saveliev G. Using microlepton methods in searching for minerals, monitoring catastrophes, registering harmful substances, predicting the failure of hazardous industrial facilities (rus). Int. Conf. on the safety of nuclear energy. 2009; Batiliman.



- Greig O. Psychics and magicians serving in the special services (rus). Algorithm, Moscow. 2012.
- Hachumova K, Surinov B, Voekov V, Germanov E, Fedorenko A. Technology that challenges current thinking: transfer of properties of medical drugs via lines of communication (rus). *Int. J. of Unconventional Science* 2014; 5(2): 08–117.
- Hansel C. Extra-Sensory Perception. A scientific evaluation. NY Chales Scribner's sons. 1969.
- Hirukawa T and Ishikawa M. Anomalous fluctuation of RNG data in Nebula: Summer festival in northeast Japan. The Parapsychological Association Convention 2004; pp: 389–297.
- Interfax. The military environment of Yeltsin used the 'psi-services' from the General Staff of the RF (rus). Interfax, 13 September. 2007.
- Jedlicka P. Revisiting the quantum brain hypothesis : toward quantum (neuro)biology? *Frontiers in molecular neuroscience* 2017; 10(Art. 366): 1 – 8.
- Kernbach S. Exploration of high-penetrating capability of LED and laser emission. Parts 1 and 2 (rus). *Nano- and microsystem's technics* 2013a; 6,7:38–46,28–38.
- Kernbach S. Replication attempt: Measuring water conductivity with polarized electrodes. *Journal of Scientific Exploration* 2013b; 27(1):69–105.
- Kernbach S. Supernatural. Scientifically proven facts (rus). Algorithm. Moscow. 2015.
- Kernbach S. Replication experiment on distant influence on biological organisms conducted in 1986. *IJUS*, 2017a; E2(4): 41–46.
- Kernbach S. Tests of the circular Poynting vector emitter in static E/H fields. *Int. J. of Unconventional Science* 2017b; E2: 23–40.
- Kernbach S. Monitoring of remote objects (rus). *IJUS* 2018a; 21–22(6):28–42.
- Kernbach S. Spiritus mundi: Immortality project of the richest man on earth (rus). *IJUS* 2018b; 21–22(6):49–85.
- Kernbach S, Kernbach A, Rusanov A, Volkov I. Analysis of the ochatrin's detector and the smal akimov's generator. *IJUS* 2015; 9(3): 70–89.
- Kernbach S, Kuksin I, Kernbach O. On accurate differential measurements with electrochemical impedance spectroscopy. *WATER* 2017; 8: 136–155.
- Kernbach S, Zamsha V, Kravchenko Y. Experimental approach towards long-range interactions from 1.6 to 13798 km distances in bio-hybrid systems. *NeuroQuantology* 2016; 14(3): 456–476.
- Kernbach S and Zhigalov V. Report on experiments with the 'phantom effect' (rus). *IJUS* 2013; 1(2):56–60.
- Klimov PV, Falk AL, Christle DJ, Dobrovitski VV, Awschalom DD. Quantum entanglement at ambient conditions in a macroscopic solid-state spin ensemble. *Science Advances* 2015; 1: e1501015–e1501015.
- Koch C and Hepp K. Quantum mechanics in the brain. *Nature* 2006; 440: 611.
- Korotaev S, Budnev N, Serdyuk V, Kiktenko E, Gorohov J, Zurbanov V. Macroscopic entanglement and time reversal causality by data of the baikal experiment. *J. of Physics: Conference Series* 2018; 1051: 012019.
- Krasnobrygev V. Distant transmission of vaccines (rus). *Proc. of the 1st int. conf. 'Torsion fields and information interactions'* 2009; pp: 525–529.
- Kravchenko Y and Kalaschenko N. On registration of electromagnetic emission of the human body for medical diagnostics (rus). *Parapsychology and Psychophysics* 1994; 4(16): 67–80.
- Lee K, Sprague M, Sussman B, Nunn J, Langford N, Jin X, Champion T, Michelberger P, Reim K, England D, Jaksch D, Walmsley I. Entangling Macroscopic Diamonds at Room Temperature. *Science* 2011; 334(6060): 1253–1256.
- Marletto C, Coles DM, Farrow T, Vedral V. Entanglement between living bacteria and quantized light witnessed by rabi splitting. *Journal of Physics Communications*, 2018; 2(10): 101001.
- Maslobrod S. Effect of a long range interaction appeared between germinating seeds. *Maize Genetic Cooperation Newsletter* 2012; 48(6): 99–113.
- Maslobrod S, Ganea A, Corlateanu L. 'Memory' of the system of two swelling seeds of maize and distant transmission of structural bioisomerism from one seedling to other determined by this 'memory' under stress conditions. *Maize Genetic Cooperation Newsletter* 2004; 78: 11–12.
- Maslobrod S, Kernbach S, Maslobrod E. Nonlocal interactions in the system 'Digital representation of phytoobject – phytoobject'. Part 1 (rus). *Int. J. of Unconventional Science* 2014a; 4(2): 26–46.
- Maslobrod S, Kernbach S, Maslobrod E. Nonlocal interactions in the system 'Digital representation of phytoobject – phytoobject'. Part 2 (rus). *Int. J. of Unconventional Science* 2014b; 5(2): 56–78.
- Maslobrod S, Shambala S, Tretjkov N. The effect mirror symmetrization of cenotic couple of seedlings and electromagnetic interaction of germinating seeds (rus). *Doklady AN Rossii*, 1994; 334(3): 396–398.
- May EC, Rubel V, Auerbach L. *ESP WARS: East and West: An Account of the Military Use of Psychic Espionage As Narrated by the Key Russian and American Players*. CreateSpace Independent Publishing Platform. 2014
- Melkikh AV. Quantum field theory solves the problem of the collapse of the wave function. *arXiv e-prints*, 2013; arXiv:1311.0205.
- Mohseni M, Omar Y, Engel G, Plenio M. *Quantum Effects in Biology*. Cambridge University Press.
- Montagnier L, Aissa J, Giudice ED, Lavallee C, Tedeschi A, Vitiello G. (2011). DNA waves and water. *J. of Physics: Conference Series* 2014; 306(1): 012007.
- Mothersill C, Smith R, Wang J, Rusin A, Fernandez-Palomo C, Fazzari J, Seymour C. Biological entanglement-like effect after communication of fish prior to x-ray exposure. *Dose-Response* 2018; 16: 155932581775006.



- Nelson D, Radin D, Shoup R, Bancel P. Correlation of continuous random data with major world events. Technical Note PEAR 95004. 1995.
- Nelson R, Jahn R, Dunne B, Dobyns Y, Bradish G. FieldREG II: Consciousness field effects: Replications and explorations. *J of Scientific Exploration* 1998; 12(3): 425–454.
- Newsru. A special department for 'psi-safety' of the president has been disbanded in the Kremlin (rus). newsru.com: 12 January 2005.
- Ochatrin A, Ochatrin A, Sizov V. Patent RU2113000. Method to search for mineral deposits based on their own emission, a device for its implementation and microlepton indicator (rus), 21.07.1997.
- Ockeloen-Korppi CF, Damskagg E, Pirkkalainen JM, Clerk AA, Massel F, Woolley MJ, Sillanpaa MA. Stabilized entanglement of massive mechanical oscillators. *Nature* 2018; 556:062116.
- Palomaki TA, Teufel JD, Simmonds RW, Lehnert KW. Entangling mechanical motion with microwave fields. *Science* 2013; 342(6159): 710–713.
- Peng G and Kernbach S. External qi and torsion field. Somatic Science Conference (devoted to Xuesen Qian), China. 2018.
- Persinger M and Dotta B. Temporal patterns of photon emissions can be stored and retrieved several days later from the "same space": Experimental and quantitative evidence. *NeuroQuantology* 2011; 9: 605–613.
- Persinger M and Lavallee C. Theoretical and experimental evidence of macroscopic entanglement between human brain activity and photon emissions: Implications for quantum consciousness and future applications. *J Cons Explor Res* 2010; 1: 785–807.
- Popov N. Military Psychotronics - the science of witchcraft (rus). Tver. 2012.
- Press WH, Teukolsky SA, Vetterling WT, Flannery BP. Numerical Recipes in C (2Nd Ed.): The Art of Scientific Computing. Cambridge University Press, New York, NY, USA. 1992.
- Ptichkin S. Secret number 10003 (rus). *Rossiyskaya gazeta* N5078 (254), 30.12.2009.
- Qian Z, Kanzhen J, Shuduo F. The anti-senility effect of the young plant's biotic field on the aged mice (in Chinese with English abstract). *J. of China Medical University* 1994; 23: 6.
- Radin D. Exploring relationships between random physical events and mass human attention: Asking for whom the bell tolls. *J. of Scientific Exploration* 2002; 16(4): 533–547.
- Russell EW. Report on Radionics. Saffron Walden: The C. W. Daniel Company Limited. 1997.
- Schmieke M. Der zweite Weg: Mein Leben im Informationsfeld. Neomedica. 2015.
- Shi S, Kumar P, Lee KF. Generation of photonic entanglement in green fluorescent proteins. In *Nature Communications* 2017; 8: 1934.
- Shkatov V. Remote monitoring of a person by his photo (rus). Proc. of Int. Conf. 'Bioenergoinformation interactions - unity and harmony of the world', Moscow, 2010; pp: 74–81.
- Smirnov A. Long-range nonlocal interactions in 'teleportation' of information (rus). Proc. of II Int. Conf. 'Torsion fields and information interactions' 2010; pp: 119–149.
- Sperling J and Walmsley IA. Entanglement in macroscopic systems. *Phys Rev A* (2017); 95: 062116.
- Surinov B. Ultra-weak emissions and feature modelling of biologically active substances. Overview (rus). In *Radiation and risk. Bulletin of the National Radiation Epidemiological Registry* 2018; 27:2, pp: 28-36.
- Swann I. Natural ESP. Bantam. 1987.
- Vedral V. Quantifying entanglement in macroscopic systems. *Nature* 2008; 453(7198): 1004–1007.
- Wang M, Lü XY, Wang YD, You JQ, Wu Y. Macroscopic quantum entanglement in modulated optomechanics. *Phys Rev A* 2016; 94: 053807.
- Yan X, Lin H, Li H, Traynor-Kaplan A, Xia ZQ, Fang FLY, Dao M. Structure and property changes in certain materials influenced by the external qi of qigong. *Mat Res Innovat* 1999; (2): 349–359.
- Zhigalov V. Can we control the collapse of wave function? Part 1. *Int. J. of Unconventional Science* 2016; 4(4): 82–89.

